

DOE/BC/15112-2  
(OSTI ID: 775023)

OPTIMIZATION OF SURFACTANT MIXTURES AND THEIR  
INTERFACIAL BEHAVIOR FOR ADVANCED OIL RECOVERY

Annual Report  
February 2001

By  
Prof. P. Somasundaran

Date Published: February 2001

Work Performed Under Contract No. DE-AC26-98BC15112

Columbia University in the city of New York  
New York, New York



**National Energy Technology Laboratory  
National Petroleum Technology Office  
U.S. DEPARTMENT OF ENERGY  
Tulsa, Oklahoma**

## **DISCLAIMER**

This report was prepared as an account of work sponsored by an agency of the United States Government. Neither the United States Government nor any agency thereof, nor any of their employees, makes any warranty, expressed or implied, or assumes any legal liability or responsibility for the accuracy, completeness, or usefulness of any information, apparatus, product, or process disclosed, or represents that its use would not infringe privately owned rights. Reference herein to any specific commercial product, process, or service by trade name, trademark, manufacturer, or otherwise does not necessarily constitute or imply its endorsement, recommendation, or favoring by the United States Government or any agency thereof. The views and opinions of authors expressed herein do not necessarily state or reflect those of the United States Government.

This report has been reproduced directly from the best available copy.

DOE/BC/15112-2  
Distribution Category UC-122

Optimization of Surfactant Mixtures and Their Interfacial Behavior for Advanced Oil Recovery

By  
Prof. P. Somasundaran

February 2001

Work Performed Under Contract DE-AC26-98BC15112

Prepared for  
U.S. Department of Energy  
Assistant Secretary for Fossil Energy

Jerry Casteel, Technology Manager  
National Petroleum Technology Office  
P.O. Box 3628  
Tulsa, OK 74101

Prepared by  
Columbia University in the city of New York  
Box 20, Low Memorial Library  
New York, NY 10027

## TABLE OF CONTENTS

	Page
LIST OF FIGURES .....	v
LIST OF TABLES .....	vii
EXECUTIVE SUMMARY .....	ix
MATERIALS & METHODS .....	1
Materials .....	1
N-alkyl-2-pyrrolidones .....	2
Sugar-based Surfactants .....	3
Mineral Samples .....	4
Other Chemicals .....	5
Methods .....	5
Analytical Techniques .....	5
Adsorption .....	6
Surface tension .....	6
Zeta potential .....	6
Fluorescence spectroscopy .....	7
RESULTS & DISCUSSION .....	9
Phase Separation, Surface Activity And Micellization in Mixtures of N-hexyl 2-pyrrolidone And Water .....	9
Micellization Behavior of N-cyclohexyl-2-pyrrolidone .....	16
Adsorption of N-dodecyl- $\beta$ -d-maltoside on Various Hydrophilic Solids .....	29
Alkyl Glucosides And Alkyl Maltosides at The Solid/liquid Interfaces .....	31
Adsorption of Alkyl Glucosides and Alkyl Maltosides on Alumina .....	31

Adsorption Kinetics of N-Dodecyl- $\beta$ -D-Maltoside on Alumina .....	33
Effect of pH on the N-Dodecyl- $\beta$ -D-Maltoside Adsorption .....	34
Effect of Salt on the N-Dodecyl- $\beta$ -D-Maltoside Adsorption .....	35
Fluorescence Spectroscopic Study on N-Dodecyl- $\beta$ -D-Maltoside Adsorption ..	36
Effect of Temperature on the Adsorption of N-Dodecyl- $\beta$ -D-Maltoside on Alumina .....	37
Hydrophobicity of Alumina with N-Dodecyl- $\beta$ -D-Maltoside Adsorption .....	39
 PUBLICATION .....	 42

## LIST OF FIGURES

	Page
<b>Figure 1</b>	<b>The structure of Alkyl xylene sulfonate . . . . . 1</b>
<b>Figure 2</b>	<b>The Structure of N-alkyl-2-pyrrolidone . . . . . 3</b>
<b>Figure 3</b>	<b>The Chemical Structures and Molecular Models of a) n-octyl-<math>\beta</math>-D-glucoside b) n-dodecyl-<math>\beta</math>-D-maltoside . . . . . 4</b>
<b>Figure 4</b>	<b>Phase Diagram of Hexyl-Pyrrolidone with Water. . . . . 9</b>
<b>Figure 5</b>	<b>Interfacial Tension in the N-Hexyl-2-Pyrrolidone/Water Two-Phase System at Different Temperatures. The LCT is indicated at zero tension. . . . . 10</b>
<b>Figure 6</b>	<b>Surface Tension of Solutions of N-hexyl-2-pyrrolidone in Water at 18 °C. 11</b>
<b>Figure 7</b>	<b>Depression of the freezing point (DT) of N-hexyl-2-pyrrolidone solutions in water . . . . . 11</b>
<b>Figure 8</b>	<b>Solubility of pyrene in N-Hexyl-2-Pyrrolidone/Water mixtures at 20 °C . . . 12</b>
<b>Figure 9</b>	<b>Phase diagram of N-hexyl-2-pyrrolidone in water including micelle formation and ice separation . . . . . 13</b>
<b>Figure 10</b>	<b>Surface Pressure of the Mixtures of N-Hexyl-2-Pyrrolidone in Water at 25 °C . . . . . 14</b>
<b>Figure 11</b>	<b>Surface pressure-area isotherm for N-hexyl-2-pyrrolidone adsorbed from aqueous solutions at 25° C . . . . . 15</b>
<b>Figure 12</b>	<b>Surface tension of CHP aqueous solutions at 21 °C using Drop Volume Method . . . . . 17</b>
<b>Figure 13</b>	<b>Surface tension of CHP at different temperatures using plate and drop volume methods. . . . . 18</b>
<b>Figure 14</b>	<b>Pyrene solubility in CHP/Water mixtures . . . . . 18</b>
<b>Figure 15</b>	<b><math>I_3/I_1</math> ratio of pyrene fluorescence spectrum in cyclohexyl pyrrolidone aqueous solution . . . . . 19</b>
<b>Figure 16</b>	<b>Freezing point depression of cyclohexyl pyrrolidone aqueous solutions . . . 20</b>
<b>Figure 17</b>	<b>Surface pressure of cyclohexyl pyrrolidone at the air/water interface. . . . 22</b>
<b>Figure 18</b>	<b><math>\Pi/C</math> as a function of concentration of cyclohexyl pyrrolidone in water . . . 23</b>

<b>Figure 19</b>	<b>Heat capacity of cyclohexyl pyrrolidone/water mixtures at 25 °C</b> . . . . .	<b>24</b>
<b>Figure 20</b>	<b>Heat of dilution of cyclohexyl pyrrolidone in water</b> . . . . .	<b>26</b>
<b>Figure 21</b>	<b>Partial molar heat of dilution of cyclohexyl pyrrolidone in water at the 24 °C</b> . . . . .	<b>27</b>
<b>Figure 22</b>	<b>Relative viscosities of CHP/water mixture at 25 °C.</b> . . . . .	<b>28</b>
<b>Figure 23</b>	<b>Adsorption Isotherms of N-Dodecyl-β-D-Maltoside on Hydrophilic Solids</b> .	<b>30</b>
<b>Figure 24</b>	<b>Adsorption of N-Alkyl-β-D-Glucosides on Alumina</b> . . . . .	<b>31</b>
<b>Figure 25</b>	<b>Adsorption of N-Alkyl-β-D-Maltosides on Alumina</b> . . . . .	<b>32</b>
<b>Figure 26</b>	<b>Adsorption Kinetic of N-Dodecyl-β-D-Maltoside on Alumina</b> . . . . .	<b>33</b>
<b>Figure 27</b>	<b>Effect of pH on the Adsorption of N-Dodecyl-β-D-Maltoside on Alumina</b> .	<b>34</b>
<b>Figure 28</b>	<b>Effect of Salt (Na<sub>2</sub>SO<sub>4</sub>) on the Adsorption of N-Dodecyl-β-D-Maltoside on Alumina</b> . . . . .	<b>35</b>
<b>Figure 29</b>	<b>Polarity parameters of Pyrene at the Alumina/Water Interface and in Supernatant As a Function of N-Dodecyl-β-D-Maltoside Adsorption</b> . . . .	<b>37</b>
<b>Figure 30</b>	<b>Effect of Temperature on the Adsorption of N-Dodecyl-β-D-Maltoside on Alumina</b> . . . . .	<b>38</b>
<b>Figure 31</b>	<b>Adsorption of N-Dodecyl-β-D-Maltoside and Its Effect on the Hydrophobicity of Alumina Particles as Determined by Two Phase Separation</b> . . . . .	<b>39</b>
<b>Figure 32</b>	<b>Hydrophobicity of Alumina Particles after N-Dodecyl-β-D-Maltoside Adsorption</b> . . . . .	<b>41</b>

## LIST OF TABLES

	Page
<b>Table I</b> Surfactants Used And Their Molecular Structure .....	2
<b>Table II</b> List of Alkyl Polyglucoside Surfactants Used .....	3
<b>Table III</b> List of Solids Used .....	5



## EXECUTIVE SUMMARY

The aim of this research is to develop improved extraction processes to mobilize and produce the oil left untapped using conventional techniques. Current chemical schemes for recovering the residual oil have been in general less than satisfactory. High cost of the processes as well as significant loss of chemicals by adsorption on reservoir minerals and precipitation has limited the utility of chemical-flooding operations. There is a need to develop cost-effective, improved reagent schemes to increase recovery from domestic oil reservoirs. It is our aim to develop and evaluate novel mixtures of surfactants for improved oil recovery. Emphasis will be placed on designing cost-effective processes compatible with existing conditions and operations in addition to ensuring minimal reagent loss. The advantage of using surfactant mixtures is that interfacial behavior of such mixtures can be synergistic (or antagonistic) and can be manipulated by adjusting surfactant type and properties, such as mixing ratio and the order of addition. It is to be noted that the past fundamental work in these systems has been mostly using single surfactants while commercial systems invariably are mixtures.

During the first year of this project, research on the interfacial behavior of pyrrolidones and sugar-based surfactants, has been initiated. Both of these reagents have the major advantage that they are environmentally benign. However the effect of structures of these compounds on their interfacial behavior such as adsorption is not known. Alkyl pyrrolidones comprise a class of biodegradable surface active agents with low vapor pressure and low toxicity, which are partially or completely miscible with water, depending on the chain length and the temperature. These molecules are very polar, with dipole moments close to 4 debye and will dissolve a variety of electrolytes. Pyrrolidones have been used in the petrochemical industry for several years mainly due to their selective affinity for unsaturated carbons, aromatics and sulfur bearing gases. These agents are particularly effective

for removing asphaltic constituents from crude oil before distillation and purification. A major aim of our current research is to systematically investigate the micro and nanocharacteristics of alkyl pyrrolidones as a function of surfactant structure, especially in mixtures with other components, so that their interfacial behavior as surfactants in enhanced oil recovery (EOR) can be optimized

As part of our effort to study mixed surfactants, we investigated the interfacial and micellization behavior of N-hexyl 2-pyrrolidone (HP). The results show that N-hexyl 2-pyrrolidone (HP) and water are partially miscible above a lower consolute temperature (LCT) of 19.1 °C. The interfacial tension of this two phase system was measured as a function of temperature. HP is surface active at the air/solution interface and forms micelles in solution at all temperatures ranging from the freezing point up to the LCT and up to 25 °C in the water-rich phase above the LCT. At low water contents, water is positively adsorbed at the air/solution interface. These results are very important to design the interfacial behavior of the surfactants during the process of enhanced oil recovery. To better understand structure-performance relationship, the aggregation of another pyrrolidone surfactant, N-cyclohexyl-2-pyrrolidone (CHP), in aqueous solution and its adsorption at the air/solution interface were also studied, using surface tension, pyrene solubilization, fluorescence, viscosity, freezing point, and calorimetric techniques. It was found that CHP molecules form small micelles in water at a relatively high c.m.c. (0.45 M). The interior of the micelle is more polar than that of the common long-chain surfactants such as sodium dodecyl sulfate (SDS). This compares with the behavior of hexyl pyrrolidone micelles. At high CHP/H<sub>2</sub>O ratios the large exothermic heats of mixing suggest hydrate formation. The partial molar heats of dilution in the micellar range indicate that the micellar structure changes significantly with concentration. The two-dimensional second virial coefficient of the adsorbed monolayer of CHP at the air/water interface, estimated using the surface pressure data at low CHP concentrations, becomes more negative with increase in temperature and

the standard heat of adsorption is endothermic. Surprisingly, this suggests increasing attraction between chains with increase in temperature. Implications of increase in temperature in enhanced oil recovery (EOR) on adsorption due to this should be noted.

Adsorption of n-alkyl- $\beta$ -D-glucosides and maltosides on solids was also investigated. Effect of surfactant structure as well as pH, electrolyte, temperature, solid loading, etc. on the adsorption were systematically studied. The adsorption of above surfactants on hydrophilic solids such as alumina is divided into three regions, in contrast to the four regions in the case of anionic ones. At lower concentrations, the surfactant adsorbs individually due to interactions between the surfactant head and the solid surface. At higher concentrations interactions between surfactant chains take place leading to a steep rise in adsorption. Above the cmc of the surfactant the adsorption reaches a plateau. The structure of the saturated adsorbed layer is close to that of a bilayer with hydrophobic chains interpenetrating each other.

Interestingly, the adsorption on hydrophilic solids showed the surfactant n-dodecyl- $\beta$ -D-maltoside to adsorb on alumina, hematite and titania, but much less on silica. The shapes of the adsorption isotherms for alumina, hematite, titania are quite different from that for silica. This behavior of alkyl maltoside on hydrophilic solids is opposite to that of alkyl polyethylene oxide surfactant, and this unique behavior of the sugar-based non-ionic surfactants has practical implications. Salinity has an effect on the adsorption and this is attributed to the salting out of the surfactant hydrophobic chain. In contrast, as expected for nonionic surfactants, the adsorption is not affected by the pH changes in the solution. Temperature also has a small effect on the adsorption, suggesting that there is no chemical interaction between surfactant and alumina.

On these solids the final adsorption state is the one in which the surface becomes hydrophilic or water wetted. This is supported by the results obtained for the wettability and stability changes of

the solids upon surfactant adsorption. These properties suggest the potential of N-dodecyl- $\beta$ -D-maltoside in various wetting, oil recovering, detergency, dispersion and flotation processes. As surface is wetted when fully saturated with sugar based surfactants, oil displacement can be expected to be high efficient.

## MATERIALS & METHODS

### MATERIALS

**Surfactants:** Several typical ionic and nonionic surfactants were selected for this study. Alkyl xylene sulfonates with different structures were obtained from ARCO Exploration and Technology Co. All these surfactants were specified to be at least 97% isomerically pure on the basis of NMR characterization. A typical structure of Alkyl xylene sulfonate is described in figure 1.

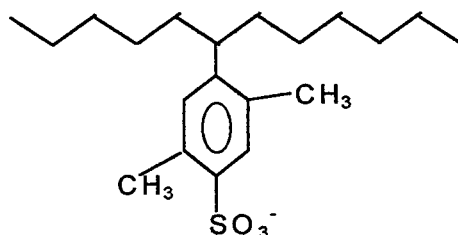


Figure 1. The structure of Alkyl xylene sulfonate

The alkyl xylene sulfonate samples received possess different chain length with 11 to 16  $\text{-CH}_2\text{-}$  groups. The position at which benzene ring is linked to the alkyl chain and the position of sulfonate group on the benzene ring is systematically varied in samples. These samples offered a unique opportunity to systematically study the effect of surfactant structures, particularly in mixed systems.

Sodium dodecyl sulfate (SDS) of greater than 99% purity purchased from Fluka chemicals was used as received. The nonionic surfactants covered a wide range of hydrophobic and hydrophilic chain lengths and were purchased from Nikko Chemicals. The ethoxylated alcohols are of the general structure  $\text{C}_n\text{H}_{2n+1}(\text{CH}_2\text{CH}_2\text{O})_m\text{H}$  or  $\text{C}_n\text{EO}_m$ , and the homologues studied are  $\text{C}_{10}\text{EO}_8$ ,  $\text{C}_{12}\text{EO}_8$ ,  $\text{C}_{14}\text{EO}_8$ , and  $\text{C}_{16}\text{EO}_8$ . This enables a study of the effect of surfactant chain length both in terms of hydrocarbon

and ethoxyl groups on adsorption of mixtures. In addition to the alcohols, nonyl phenols obtained from Barnett Products, New Jersey with different number of ethylene oxide groups will be also studied. Cationic tetradecyl trimethyl ammonium chloride (TTAC) of greater than 99% purity purchased from TCI Chemicals, Japan will be used as received. These surfactants are listed in table I.

**Table I. Surfactants used and their molecular structure**

Surfactant	molecular structure	purity
Alkyl xylene surfonates	$C_nH_{2n+1}(C_6H_2)(CH_3)_2.SO_3Na$	>97%
Sodium dodecyl sulfate	$C_{12}H_{23}.SO_4Na$	>99%
Polyethoxylated alcohol	$C_nH_{2n+1}(CH_2CH_2O)_mH$	>97%
Polyethoxylated nonyl phenol	$C_9H_{19}(C_6H_4)(CH_2CH_2O)_nH$	>97%
Tetradecyltrimethylammonium chloride	$[CH_3(CH_2)_{13}N(CH_3)_3]Cl$	>98%

#### *N-alkyl-2-pyrrolidones*

The N-alkyl-2-pyrrolidones comprise a class of biodegradable surface active solvents with low vapor pressure and low toxicity, which are partially or completely miscible with water depending on the chain length and temperature. These molecules are very polar, with dipole moments close to 4 Debye and liquid dielectric constants in the range of 32 (methyl) to 20 (dodecyl). The liquids are conducting and will dissolve a variety of electrolytes. The molecules form a resonance hybrid of a nonionic and zwitterionic molecule.

In this work, N-ethyl, butyl, hexyl, octyl, and dodecyl-2-pyrrolidones are used. The structure

of pyrrolidone is shown in figure 2:

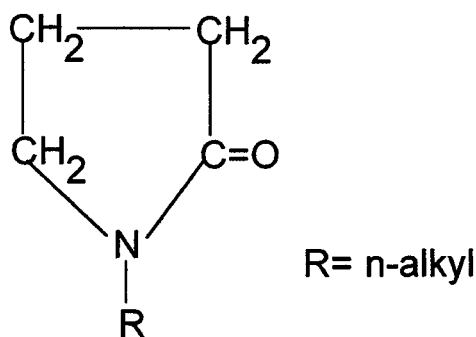


**Figure 2. The Structure of N-alkyl-2-pyrrolidone**

These compounds were analyzed by GLC. Purity of all the N-alkyl-2-pyrrolidones is greater than 99.6%. All the materials were provided by Interfacial Speciality Products Inc.

#### *Sugar-based Surfactants*

Non-ionic surfactants, n-alkyl- $\beta$ -D-glucosides and n-alkyl- $\beta$ -D-maltosides, used for this study are listed in Table II.

**Table II. List of Alkyl Polyglucoside Surfactants Used**

Name	Molecular formula	Molecular Weight	Source
n-octyl- $\beta$ -D-glucopyranoside	$C_{14}H_{26}O_6$	292.4	Calbiochem
n-nonyl- $\beta$ -D-glucopyranoside	$C_{15}H_{30}O_6$	306.4	Calbiochem
n-decyl- $\beta$ -D-glucopyranoside	$C_{16}H_{32}O_6$	320.4	Calbiochem
n-dodecyl- $\beta$ -D-glucopyranoside	$C_{18}H_{36}O_6$	348.5	Calbiochem
n-octyl- $\beta$ -D-maltoside	$C_{20}H_{38}O_{11}$	454.5	Calbiochem
n-decyl- $\beta$ -D-maltoside	$C_{22}H_{42}O_{11}$	482.6	Calbiochem
n-dodecyl- $\beta$ -D-maltoside	$C_{24}H_{46}O_{11}$	510.6	Calbiochem
n-tetradecyl- $\beta$ -D-maltoside	$C_{26}H_{50}O_{11}$	538.6	Calbiochem

The structures of n-octyl- $\beta$ -D-glucoside and n-dodecyl- $\beta$ -D-maltoside are shown in Figure 3. These surfactants were obtained in relatively pure form (>95% purity by TLC) and serve as suitable model compounds for alkyl polyglucosides. They will be used as received.

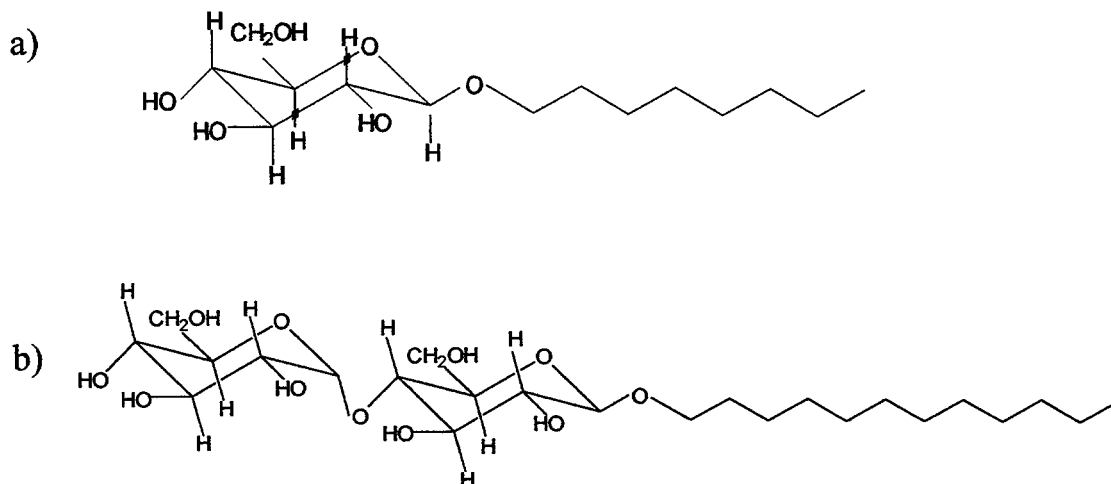


**Figure 3. The Chemical Structures and Molecular Models of a) n-octyl- $\beta$ -D-glucoside  
b) n-dodecyl- $\beta$ -D-maltoside**

*Mineral Samples:*

Solid substrates selected for this study are alumina, hematite, titania, silica and graphite which have been well characterized in the past. These solids were chosen because of their low solubility, and relatively surface homogeneity with considerable amount of information in the literature. They are listed in Table III.

**Table III. List of Solids in Used**

Name	isoelectric point (iep)	mean particle size ( $\mu\text{m}$ )	specific surface area ( $\text{m}^2/\text{g}$ )	Source
AKP-50 Alumina	8.9	0.2	10.8	Sumitomo
Silica	2	0.2	5.8	Johnson-Matthey
Silica	2	40 - 100	25	Spherosil
Titania	2	2	2.133	Alfa Products
Alumina	9.0	0.3	14	Praxair
Kaolinite	--	--	8.2	Univ. of Missouri

*Other Chemicals:*

HCl and NaOH, used for pH adjusting, from Fisher Scientific Co. were of A.C.S. grade certified (purity > 99.9%). To study the salt effects on surface tension, micellization and adsorption, LiCl, NaCl, KCl, CaCl<sub>2</sub>, AlCl<sub>3</sub>, NaF, NaSCN, Na<sub>2</sub>SO<sub>4</sub>, and Na<sub>3</sub>PO<sub>4</sub> from Fisher Scientific Co.; RbCl from Alfa Products; NaBr and NaI from Aldrich Chemical Company, Inc.; and sodium citrate from Amend Drug & Chemical Company were used as received. They are all A.C.S. certified.

Water used in all experiments was triple distilled, with a specific conductivity of less than  $1.5\mu\Omega^{-1}$  and tested for absence of organics using surface tension measurements.

Pyrene was obtained from Aldrich Chemicals and recrystallized from ethanol. NaCl, HCl and NaOH used were of ACS reagent grade. All solutions were prepared in triply distilled water and at constant ionic strength as mentioned in later sections.

**METHODS**

*Analytical Techniques:* Sodium dodecyl sulfate (SDS) concentration was determined using a two-

phase titration method<sup>1</sup>. Tetradecyl trimethyl ammonium chloride (TTAC) concentration was determined by complexing the surfactant with excess SDS and measuring the non-complexed SDS using the two-phase titration. The concentration of ethoxylated alcohol ( $C_nEO_m$ ) was determined either by total organic carbon (TOC) analysis or using high pressure liquid chromatography (HPLC) with a  $C_{18}$  bonded silica column and a refractive index detector. The solvent used was a 90:10 mixture of acetonitrile and water. Pentadecylethoxylated nonyl phenol concentration was determined by UV absorption at 223 nm.

*Adsorption:* Adsorption experiments were conducted in 25 ml Teflon capped scintillation vials. One gram of the solid was brought in contact with 5 ml of solution of desired ionic strength for 2 hours. Next, 5 ml of salt solution containing surfactant or surfactant mixture of desired concentration was added. The system was conditioned on a wrist action shaker for 15 hours in the case of silica, 24 hours in the case of alumina and 72 hours in the case of kaolinite. The suspensions were then centrifuged at 3000-4000 rpm and the supernatant analyzed for residual concentration. Adsorption was calculated based upon surfactant depleted from the solutions.

*Desorption:* The desorption tests consisted of conditioning of the supernatants of the slurries from adsorption tests for 15 hours with the desired amounts of diluents adjusted for pH and ionic strength. This procedure was repeated several times depending upon the concentration.

*Surface tension:* Surface tension of the surfactant solutions was measured using a Wilhelmy plate or a du Nuoy ring tensiometer.

*Zeta potential:* Zeta potential of mineral particles before and after adsorption were made on using Laser Zee model 501 system.

---

<sup>1</sup>Z. Li and M.J. Rosen, *Analytical Chemistry*, **53**, 1981, 1516.

*Fluorescence spectroscopy:* A Photon Technology International PTI LS-100 was used for fluorescence experiments. The samples containing pyrene dissolved to its maximum solubility in water ( $\approx 2 \times 10^{-7}$  kmol/m<sup>3</sup>) were excited at 335 nm and emission between 365 and 500 nm was recorded.



## RESULTS & DISCUSSION

### PHASE SEPARATION, SURFACE ACTIVITY AND MICELLIZATION IN MIXTURES OF N-HEXYL 2-PYRROLIDONE AND WATER

To understand the interfacial and micellization behavior of pyrrolidones, tests were done with pyrrolidones of different carbon chain length and structures. For n-hexyl 2-pyrrolidone (HP), it has

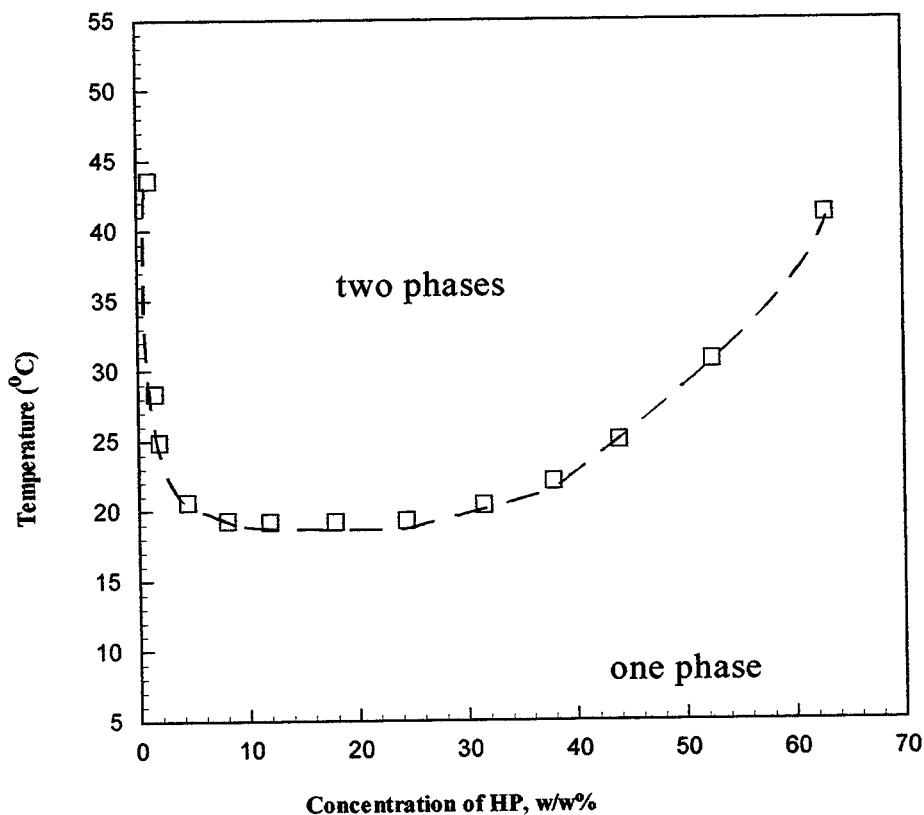


Figure 4. Phase Diagram of Hexyl-Pyrrolidone with Water

been found that it is fully miscible with water below 19.1 °C. Above this lower consolute temperature (LCT) two phases are formed (Fig.4).

The interfacial tensions ( $\sigma$ ) of the coexisting phases above the LCT are given in Fig.5, with the tension shown as zero at the LCT. Measurements of  $\sigma$  close to  $T_c$  were difficult with the

spinning drop apparatus since the drop size varies substantially with temperature, which was controlled within  $\pm 0.1$  °C. The density difference between the co-existing phases is also small at temperatures well away from  $T_c$ , making precise values of  $\sigma$  difficult to measure. The data were therefore inadequate for estimating the critical exponent for surface tension.

The surface tension at the air/solution interface at 18.°C (just below the LCT) across the whole miscible range of concentration shows a plateau region from approximately 5 to 70% (w/w), as seen in Fig.6. Above about 70 w/w% HP, the surface tension rises, indicating that water is positively adsorbed from very concentrated HP solutions. The plateau in Fig.6 indicates micellar aggregation in the solution. Micelle formation was confirmed by measurements of the freezing point

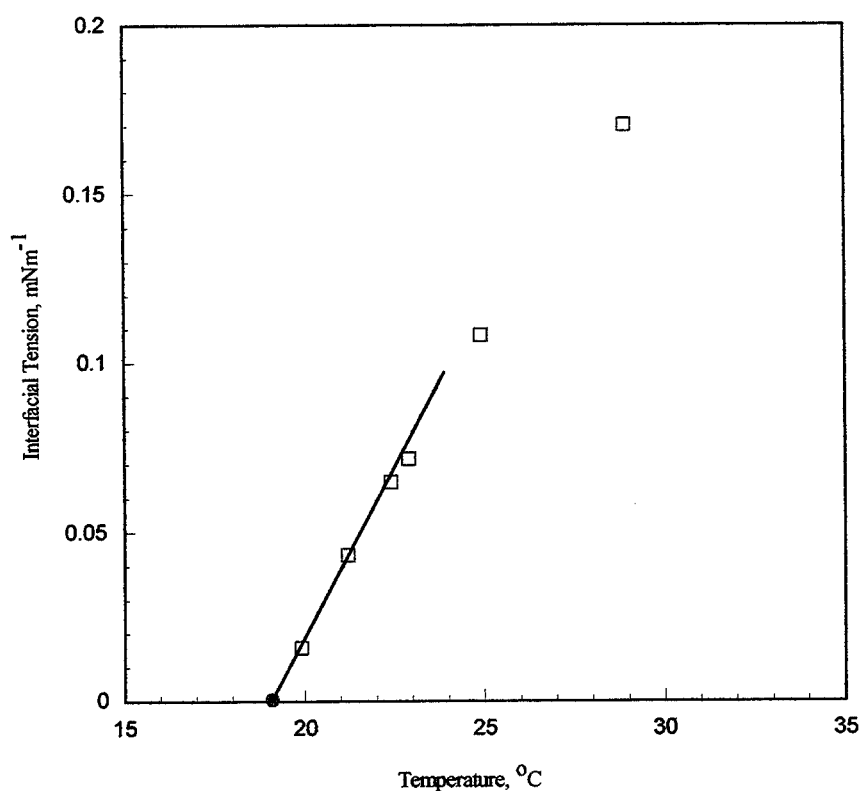


**Figure 5. Interfacial Tension in the N-Hexyl-2-Pyrrolidone/Water Two-Phase System at Different Temperatures. The LCT is indicated at zero tension.**

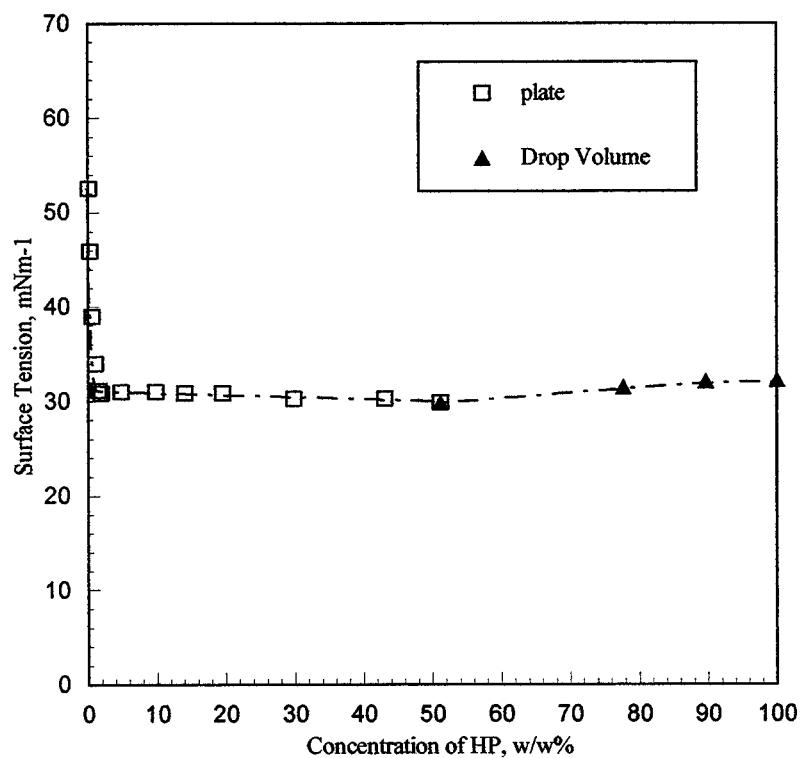


**Figure 6** Surface Tension of Solutions of N-hexyl-2-pyrrolidone in Water at 18 °C.

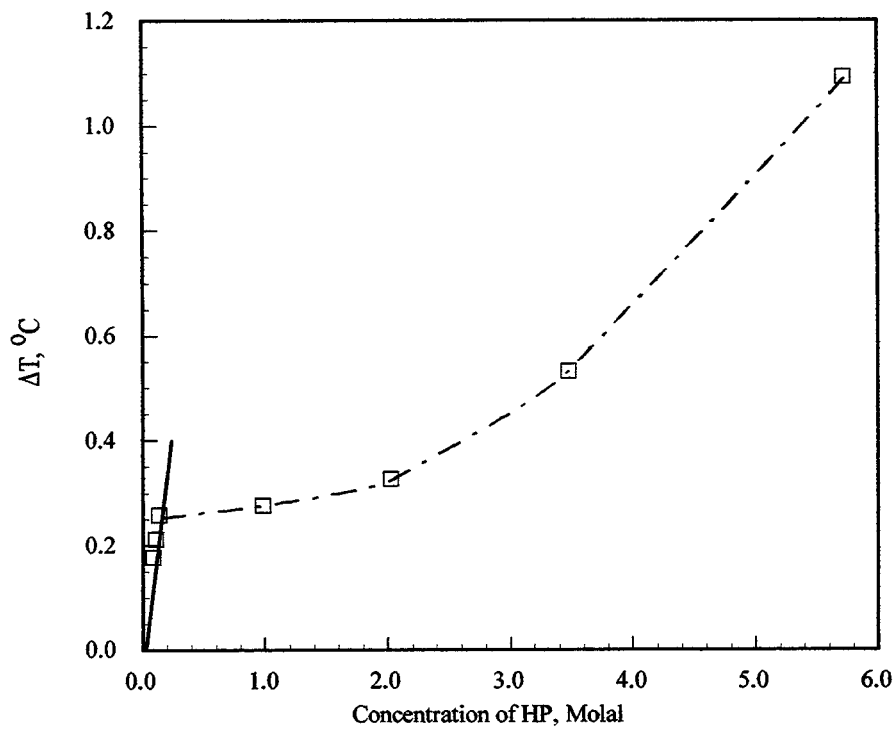


**Figure 7.** Depression of the freezing point (DT) of N-hexyl-2-pyrrolidone solutions in water

depression ( $\Delta T$ ) of water-rich mixtures, shown in Fig.7. The abrupt change in trend at 0.14 M (molal) strongly suggests micelle formation above this concentration. The aggregation number, as determined from the slope of  $\Delta T$  against concentration above the CMC, may be estimated as 80 at the freezing point.

The formation of micelles was further probed by surface tension measurements at 15 °C, and also confirmed by the large increase in the solubility of pyrene above about 0.15 M in HP/water mixtures at 20 °C shown in Fig.8. At 25 °C, the surface tension results (Fig.10) suggest micelle formation just below the saturation limit. The phase diagram in the water-rich region including micelle

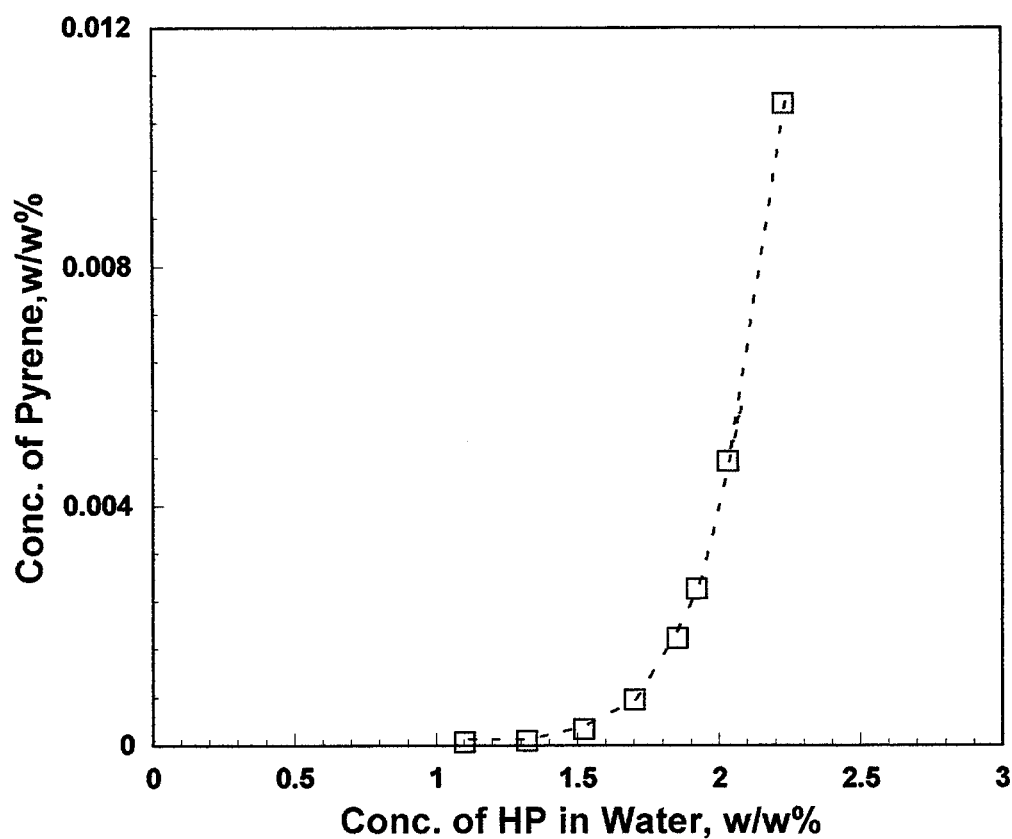
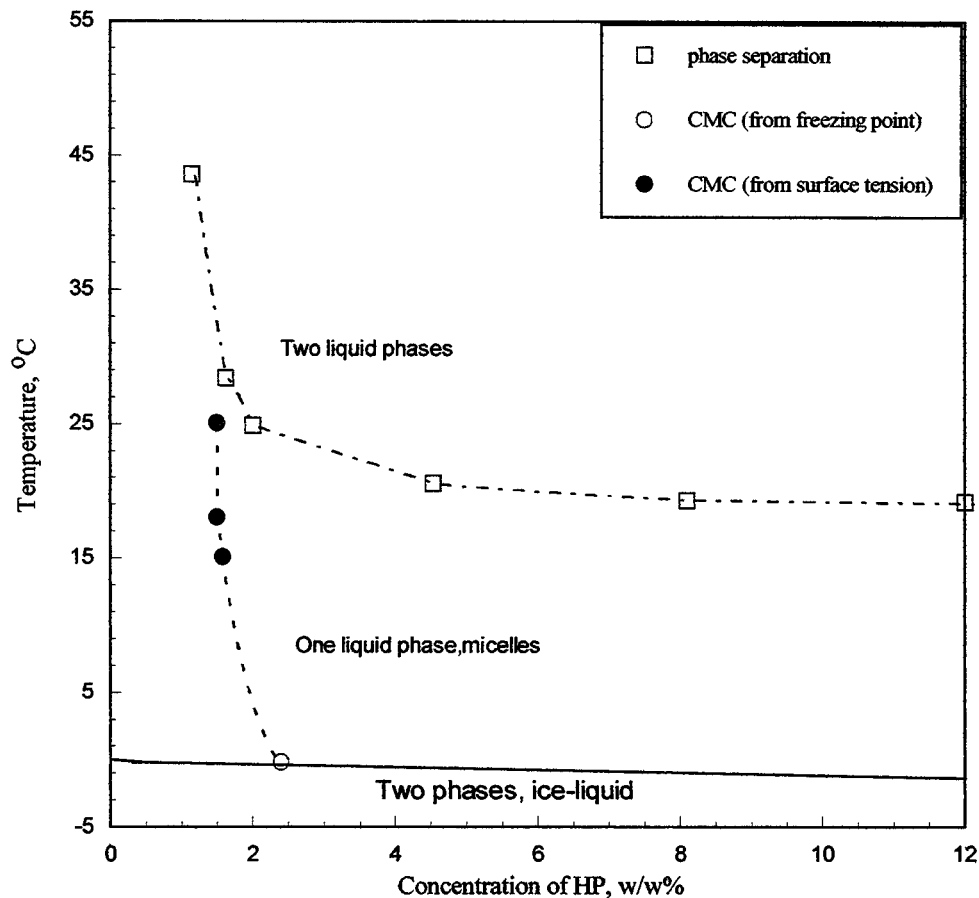


Figure 8. Solubility of pyrene in N-Hexyl-2-Pyrrolidone/Water mixtures at 20 °C



**Figure 9. Phase diagram of N-hexyl-2-pyrrolidone in water including micelle formation and ice separation**

formation and ice separation is shown in Fig.9. The CMC-temperature relationship suggests a shallow minimum in the range 15-19 °C, corresponding to a zero heat of micellization. The solubility of HP in water as a function of temperature shows an inverse Kraft point, solubility increasing as T is lowered until micelle formation begins and the solubility increases rapidly with further lowering the temperature.

From the air/water surface tension results shown in Fig.10, the excess surface density ( $\Gamma$ ) of the adsorbed HP at 25 °C close to the phase separation boundary may be calculated from the Gibbs equation in the form

$$d\Pi/d \ln a = kT\Gamma = (d \Pi/d \ln c)(d \ln c/d \ln a) \quad (1)$$

where  $\Pi$  is the surface pressure of the adsorbed HP monolayer, and  $a$  and  $c$  are the activity and concentration (molal) of HP in water. The activity coefficient ( $a/c$ ) may be estimated from the freezing point results, assuming zero heat of dilution below the CMC. The osmotic coefficients ( $g$ ) below the CMC are given within experimental error by  $g = (1-\lambda c)$ , where  $\lambda$  is  $0.5 \pm 0.05$ . The activity coefficient is related to  $g$  by  $-\ln(a/c) = 2(1-g)$ , so that

$$d \Pi/d \ln c = = kT\Gamma (1-2\lambda c) \quad (2)$$

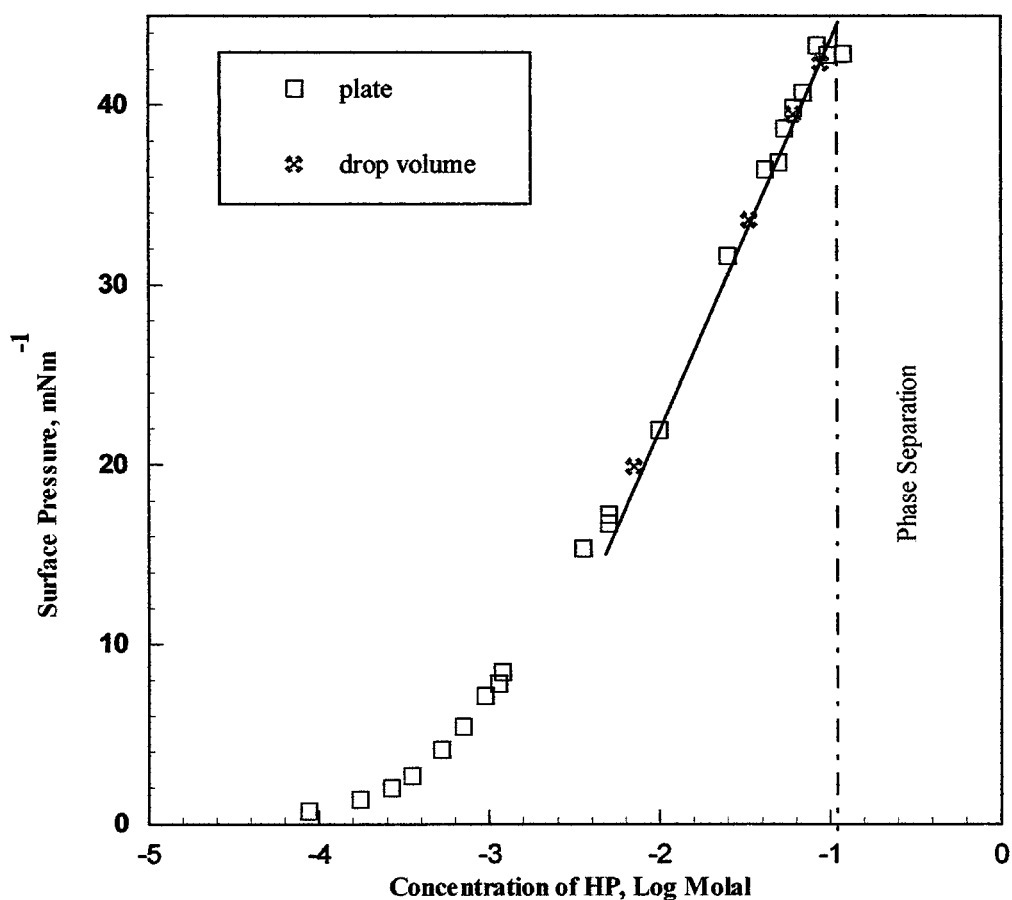


**Figure 10. Surface Pressure of the Mixtures of N-Hexyl-2-Pyrrolidone in Water at 25 °C**

In the  $\Pi$ -log  $c$  region close to the solubility limit at 25°C, the activity coefficient is not lower than 0.9, and the adsorption of HP corresponds to an area/molecule of 0.38 nm<sup>2</sup>/molecule for the N-octyl and N-dodecyl-pyrrolidones without using the activity correction at the much lower concentrations required for these two homologs. The  $\Pi$ -A (area per molecule) isotherm at 25 °C at the air/solution interface for HP is shown on Fig.11. There is no evidence for saturation adsorption at high pressures.

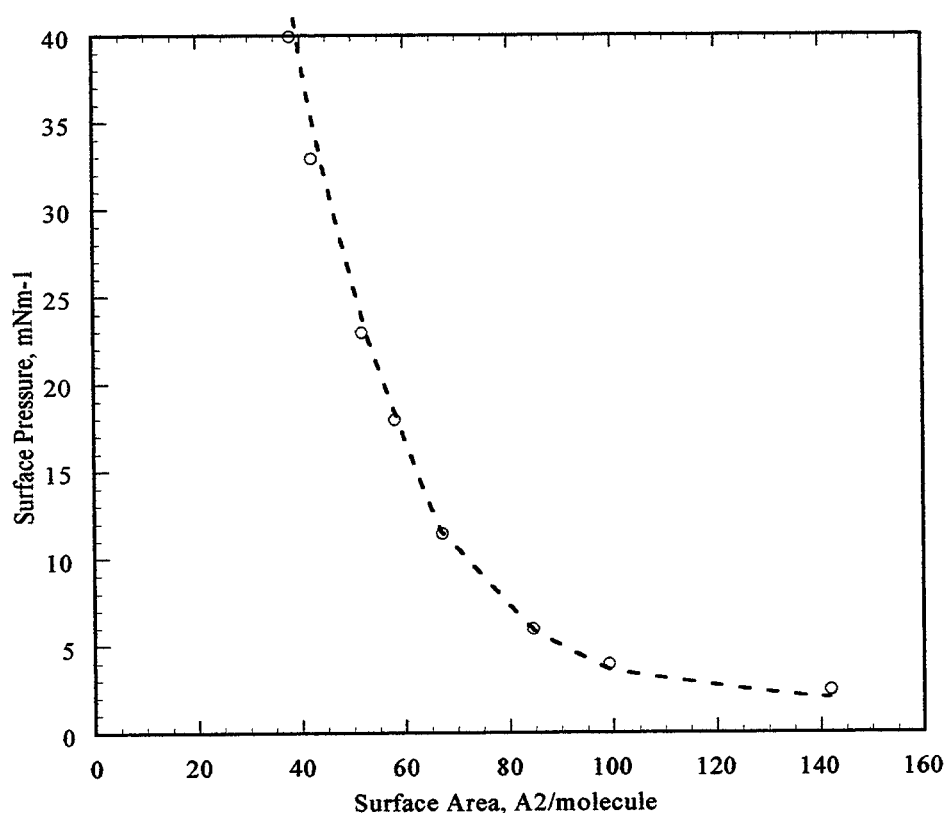


**Figure 11. Surface pressure-area isotherm for N-hexyl-2-pyrrolidone adsorbed from aqueous solutions at 25° C**

In summary, the principal findings of the current study are that N-hexyl 2-pyrrolidone in mixtures with water shows a lower consolute temperature and forms micelles over a wide concentration range. Unlike the widely studied non-ionic surfactants of the alcohol-polyoxethylene type, the phase diagram shows no sign of a closed loop (Fig.4). The existence of micellar aggregates

is clearly shown by the results for surface tension, freezing point and the pyrene solubility in HP/water mixtures. Micelles have been demonstrated at all temperatures between the freezing points and the LCT, and at temperatures up to about 25 °C in water-rich mixtures where the CMC is close to the two-phase boundary. The surface tension results for the entire concentration range below the LCT (Fig.4) show that micellar aggregates are also present in the mixtures up to about 70% HP by weight (0.2 mole fraction HP) below the LCT, and it is possible that these micelles are also present in the HP-rich one-phase region up to the phase separation temperature. At even higher concentrations of HP, the observations completed so far indicate that only water is positively adsorbed at the HP/air interface, without evidence for aqueous aggregates. Based on the high surface pressure data at the air/solution interface, the surface excess is in accord with what is expected from molecular models for the close packing.

The micellar behavior of HP and its relation to the phase diagram are similar to that found for 2-butylethanol/water mixtures, except that the HP/water phase diagram shows no closed loop for the miscibility as a function of temperature. Results of the N-substituted 2-pyrrolidones will show that micelles are formed with several compounds showing a lower consolute point with water, and that manipulation of the LCT by the addition of a third component modifies or induces micellization.

#### **MICELLIZATION BEHAVIOR OF N-CYCLOHEXYL-2-PYRROLIDONE**

Figure 12 shows the air/solution surface tension (measured by the drop volume method to avoid contact angle problems at high CHP concentrations) at  $22 \pm 0.5$  °C across the whole range of concentration. CHP is surface active, and the air/solution surface tension can be decreased to about  $40 \text{ mNm}^{-1}$  at a plateau in the range from approximately 10-60% w/w. The results suggest the formation of aggregates of CHP in solution above about 7% w/w (0.45 M). Above 60% w/w, the

surface tension decreases from the plateau value. This indicates clearly that the structure of mixtures above 60% CHP is no longer one of simple aggregates of CHP in water and that water is negatively adsorbed at high CHP ratios. Micelle formation and a critical micelle concentration (c.m.c.) of about 0.45 M are suggested more clearly on Fig. 13, which shows the surface tension plotted on a logarithmic concentration scale at two temperatures.

Micelle formation of CHP molecules in aqueous solution was confirmed by measurements of the solubility of pyrene, and of the polarity parameter ( $I_3/I_1$  ratio) in CHP aqueous solutions. Fig. 14 shows the solubility of pyrene in CHP solution. The solubility increases sharply above a concentration of about 6%, close to the c.m.c. value estimated from the surface tension results. The

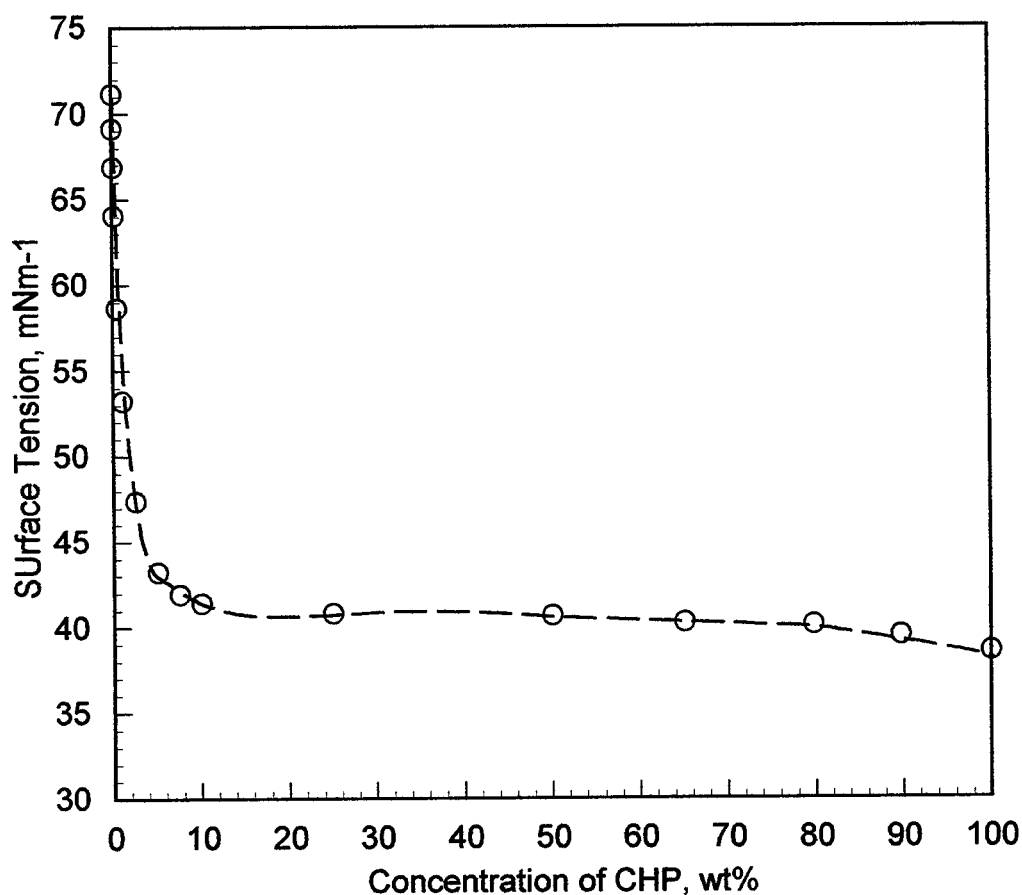


Figure 12. Surface tension of CHP aqueous solutions at 21 °C using Drop Volume Method.

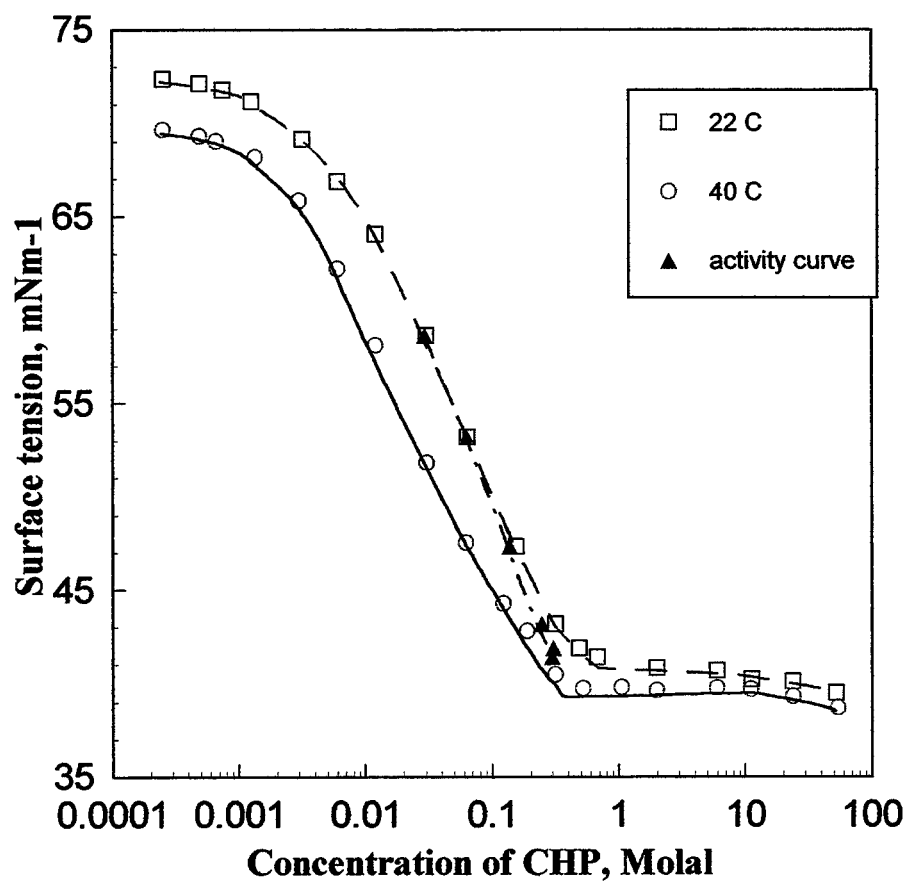


Figure 13. Surface tension of CHP at different temperatures using plate and drop volume methods.

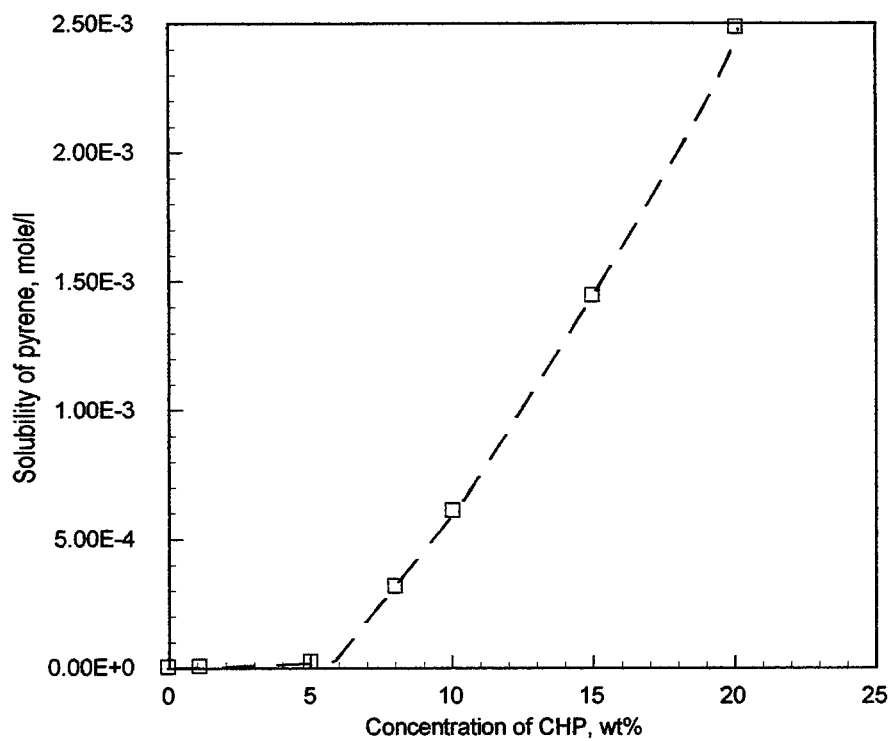


Figure 14. Pyrene solubility in CHP/Water mixtures

$I_3/I_1$  ratio of the pyrene spectrum as a function of CHP concentration in water is shown in Fig. 15 at a constant pyrene concentration of  $3 \times 10^{-7}$  M. It is seen that the ratio initially increases slightly with concentration, but with a definite change in trend over a narrow concentration range at about 6% w/w% CHP to an almost constant value of about 0.72 at high CHP concentrations. This ratio is significantly lower than that for pyrene in SDS micelles ( $\sim 0.9$ ) and similar to the ratio for dilute pyrene in pure CHP (0.73). This shows that the interior of the CHP micelle is more polar than that of the liquid paraffins which represent the interior of SDS micelles.

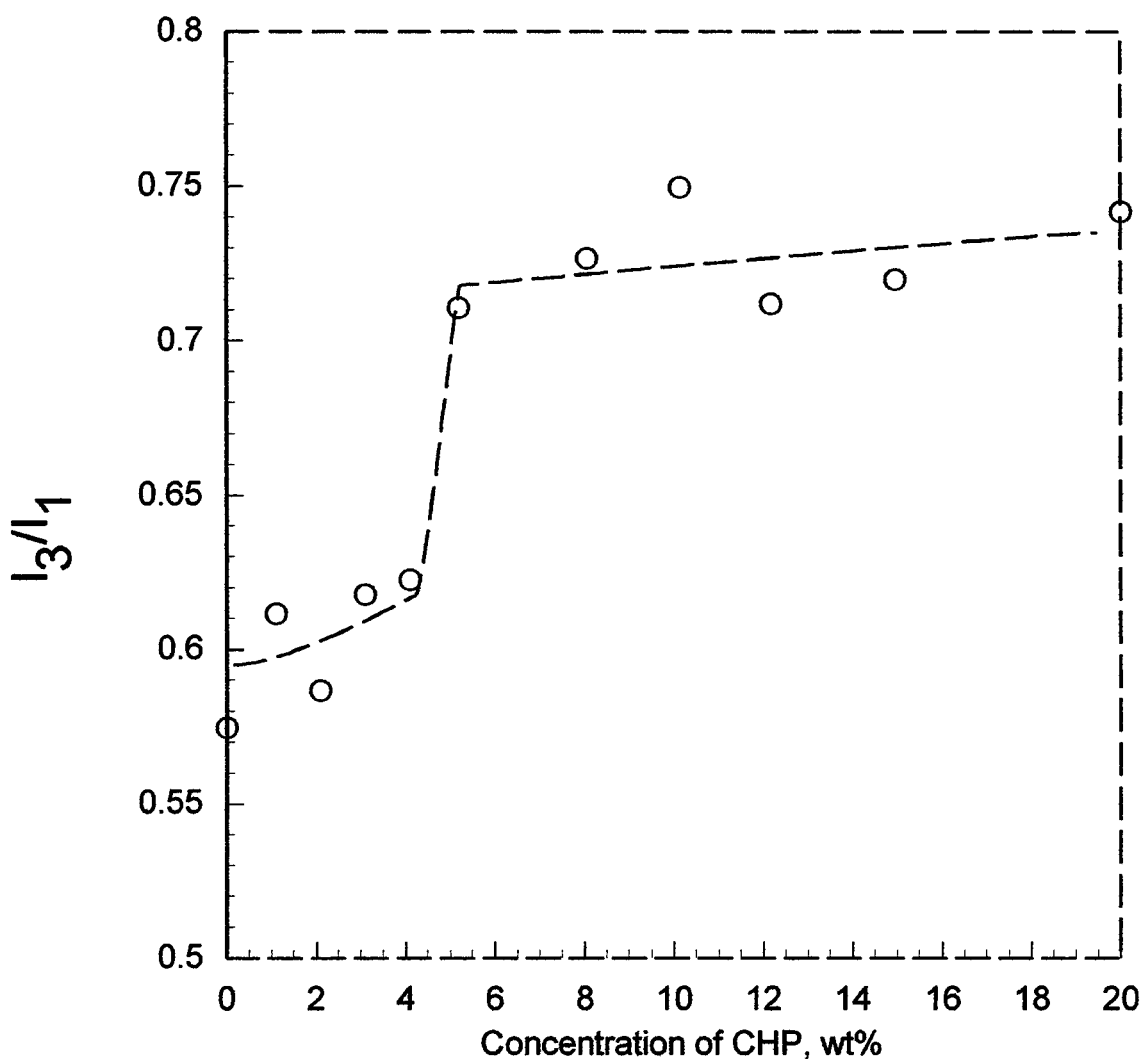
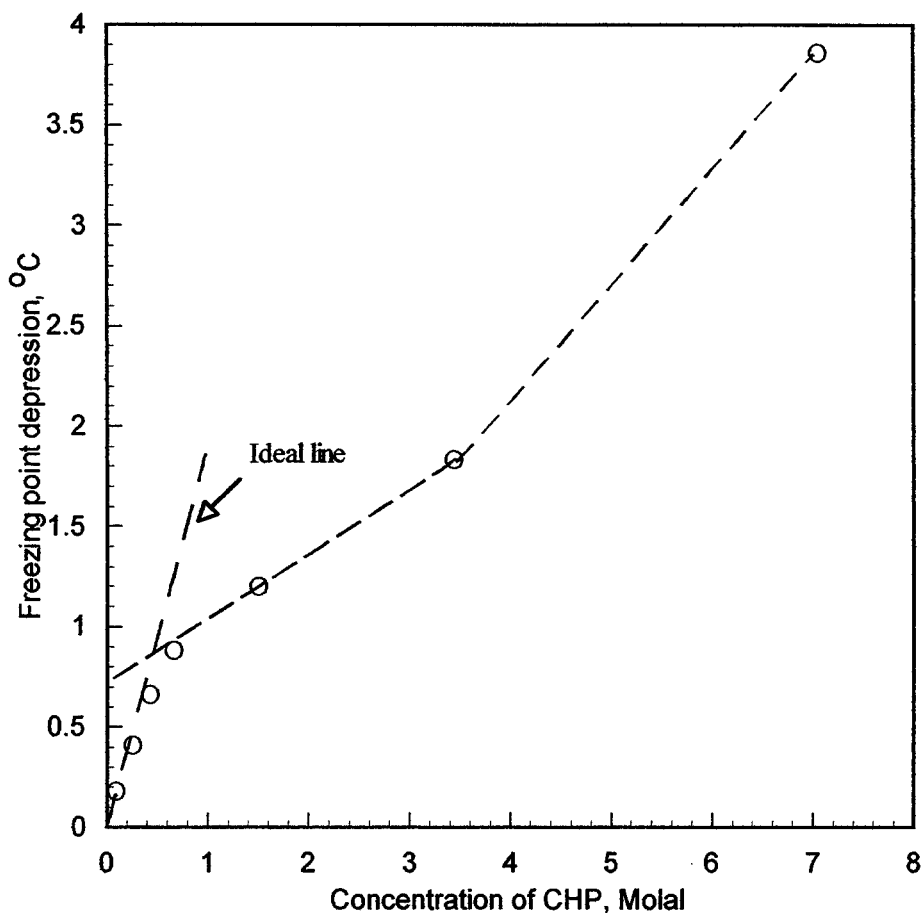


Figure 15.  $I_3/I_1$  ratio of pyrene fluorescence spectrum in cyclohexyl pyrrolidone aqueous solution

Micelle formation is also confirmed by measurements of the freezing point depression ( $\Delta T$ ) as a function of CHP concentration shown in Fig. 16. The change in trend at about 0.5 M again suggests micelle formation. The aggregation number, as judged from the slope of  $\Delta T$  against concentration above the c.m.c., may be estimated as approximately 5 at the freezing point. Approximate aggregation numbers can also be estimated from the slopes of the surface tension plots of Fig. 13 above and below the micelle point, assuming that the adsorption is constant above the c.m.c. On this basis, the aggregation number is 20-25 at 22 °C and about 70 at 40 °C, close to the lower consolute temperature. These estimates, although approximate, indicate that aggregation



**Figure 16. Freezing point depression of cyclohexyl pyrrolidone aqueous solutions**

increases with temperature. Unlike many polyoxyethylene surfactants which show lower consolute behavior, there is no “cloud point” with the alkyl pyrrolidones as the phase separation boundary is approached. The estimate of aggregation number from surface tension data at 22 °C is supported by a light scattering study using Zimm plots which gives a value of 20 at 23 °C.

### *Adsorption Behavior N-cyclohexyl-2-pyrrolidone*

The surface tension results shown in Fig. 13 at 22 °C and 40 °C show clear evidence that micellization occurs over a range of concentrations and that the c.m.c. is not a sharp transition. As described below, the activity coefficients for CHP at 22 °C in water were calculated from the freezing point and dilution heat results. The CHP activities are shown in Fig. 13 and allow direct calculation of the excess adsorption of CHP. At high surface pressures, close to the c.m.c., the adsorption corresponds to a molecular area of  $54 \pm 2 \text{ \AA}^2$  /molecule. This area is significantly higher than the  $38 \text{ \AA}^2$ /molecule at high pressure found for the N-n.hexyl-2-pyrrolidone, reflecting the effect of the cyclohexyl ring on packing in the monolayer.

The surface pressure ( $\Pi$ ) is shown in Fig.17 as a function of concentration (c) of CHP in the dilute region, and the plot of  $\Pi/c$  as a function of c is shown in Fig. 18. For monolayers, the two-dimensional virial expansion may be expressed as

$$\Pi = kT (\Gamma + B_2(T)\Gamma^2 + B_3(T)\Gamma^3 + \dots) \quad (3)$$

where  $\Gamma$  is the surface density,  $B_2(T)$ ,  $B_3(T)$ , etc. are the temperature dependent second, third, etc. virial coefficients, k is the Boltzman constant, and T is the temperature. For adsorbed monolayers, the appropriate  $\Gamma$  is the surface excess density as given by the Gibbs Adsorption Isotherm. In the dilute concentration range as shown in Fig. 17, the CHP solutions are nearly ideal. The surface excess is therefore given by

$$kT\Gamma = c \, d\Pi/dc \quad (4)$$

Combining these equations, the second virial coefficients can be expressed as

$$B_2(T) = (-\beta/\alpha^2)kT \quad (5)$$

where  $\alpha$  and  $\beta$  are the initial slopes of the  $\Pi - c$  and  $(\Pi/c) - c$  plots respectively when the concentration is close to zero.

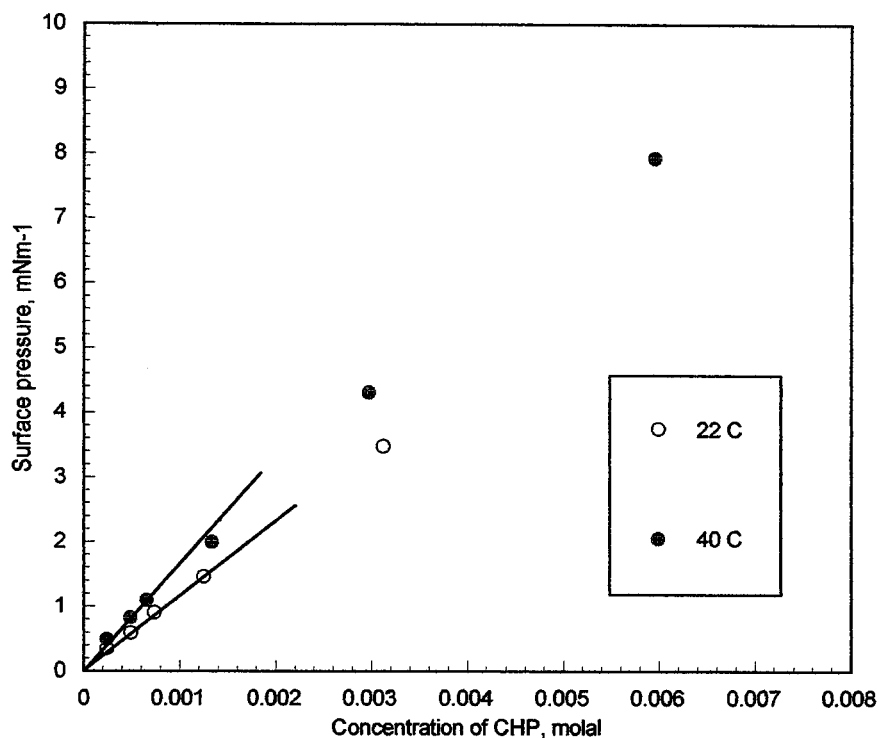


**Figure 17. Surface pressure of Cyclohexyl pyrrolidone at the air/water interface.**

Following the procedure discussed previously, the  $\alpha$  and  $\beta$  values from the lines as drawn in Figures 17 and 18 (noting that  $\alpha$  is obtainable from either  $\Pi$ - $c$  or  $\Pi/c$ - $c$  plots) are used to obtain the positive  $B_2(T)$  values at 22 ° and 40 °C of 10 Å<sup>2</sup> and 9 Å<sup>2</sup>/ molecule respectively. The data at 5° and 60 °C showed greater scatter, making estimates of  $B_2(T)$  unsatisfactory. It can be seen that the second virial coefficients become more negative with increase in temperature.

The values of  $\alpha$  as a function of temperature allow estimation of the standard heat of

adsorption of ( $\Delta H^\circ$ ) of CHP from solution to the air/water interface, using the relation

$$d(\ln \alpha)/d(1/T) = - \Delta H^\circ/R \tag{6}$$

Adsorption is endothermic with  $\Delta H^\circ$  estimated as  $11 \pm 1$  KJ/mole.

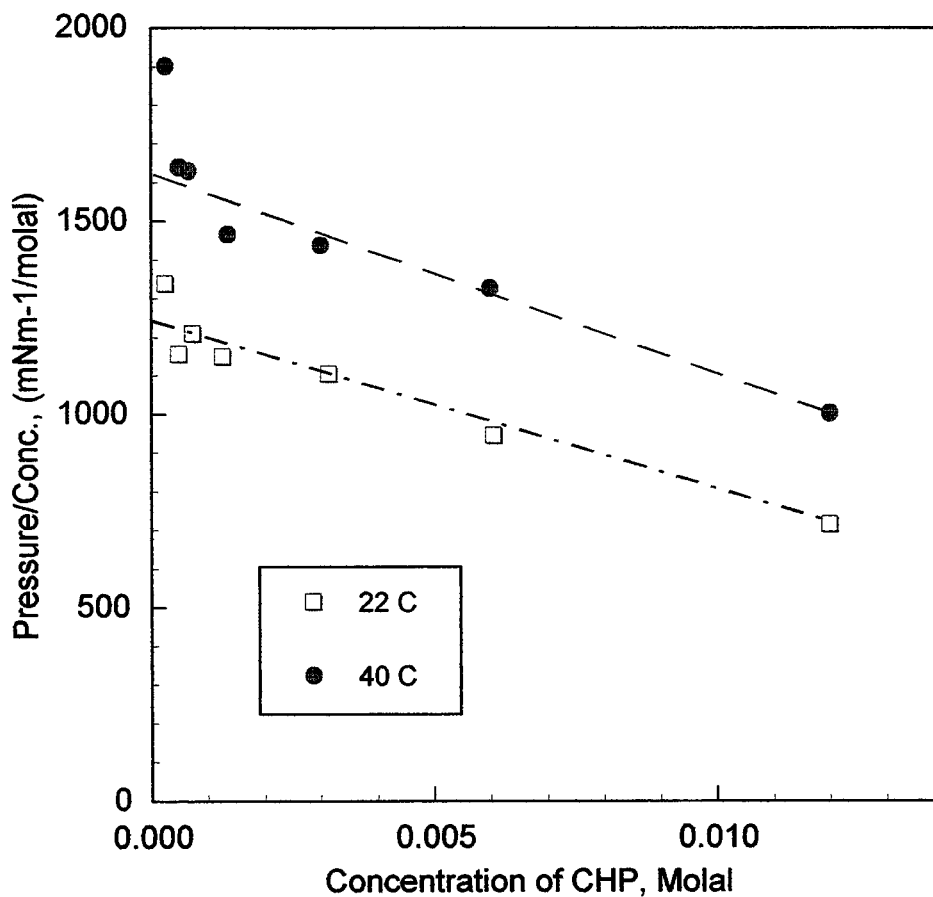
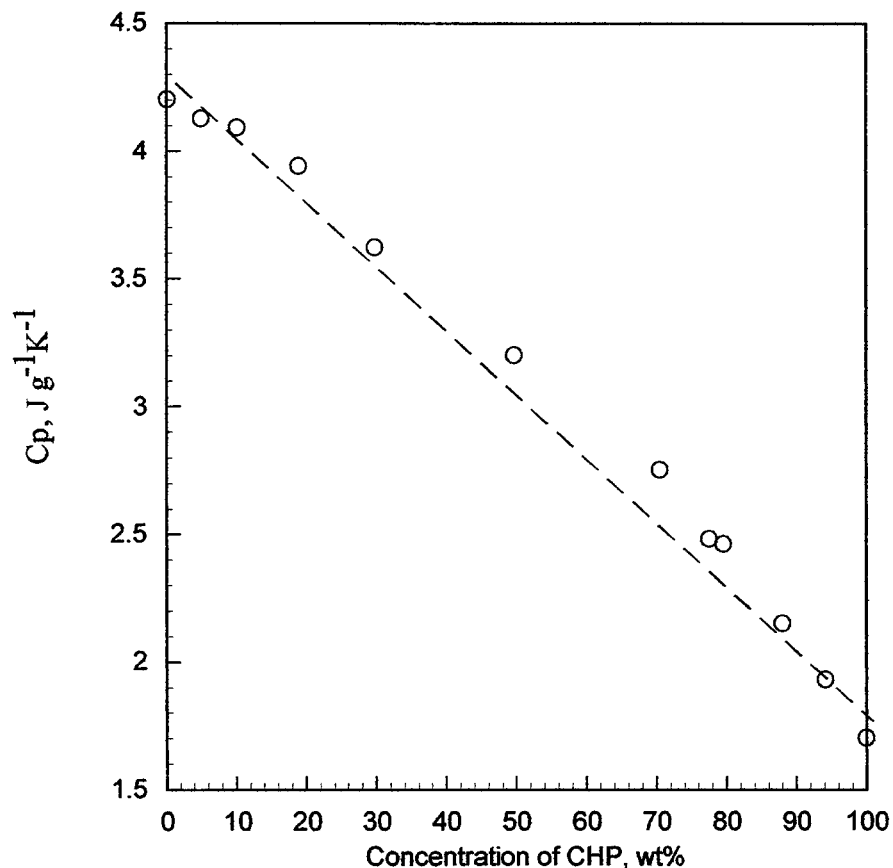


Figure 18.  $\Pi/C$  as a function of concentration of cyclohexyl pyrrolidone in water,

### Calorimetry

The heat capacities of CHP-H<sub>2</sub>O mixtures are shown in Fig. 19. The excess heat capacity of mixing is positive. The specific heat capacity of CHP is  $1.7 \text{ J g}^{-1}\text{K}^{-1}$  ( $286 \text{ J mole}^{-1} \text{ K}^{-1}$ ), well below the specific heat capacities of the n-alkanes in the same molecular weight range (decane 2.21, dodecane  $2.20 \text{ J g}^{-1}\text{K}^{-1}$ ), and close to cyclohexane (1.81), reflecting in part the restricted bond rotation

in the CHP two-ring structure. In the pure liquid state the molecules of CHP, as with other N-substituted pyrrolidones, interact strongly as shown by the high boiling point (154 °C at 7 mm Hg) and viscosity (~11.6 cp). This structuring, probably related to the interaction of the large molecular



**Figure 19. Heat capacity of cyclohexyl pyrrolidone/water mixtures at 25 °C**

dipoles, is also reflected in the low heat capacity.

The calorimetric data for the heat of mixing of CHP with water at 24 °C are shown in Figs.20 and 21. For Fig.20, the heats of dilution obtained with dilutions in the range of CHP concentrations below 50% w/w using the LKB calorimeter are added to the heat of mixing of equal masses of CHP and water (56 J g<sup>-1</sup> CHP). The overlap between the two calorimetric methods is satisfactory. Also shown in Fig. 20 is the heat of dilution at high CHP ratios on a linear scale for the addition of water.

The error introduced by the initial water content of the CHP (0.17% w/w) is minor ( $\sim 1$  J/g CHP) in reference to the precision of the measurements.

The heats of dilution show four distinct regions, best seen in Fig. 21 for the partial molar heats of dilution ( $\Delta H_d$ ). At low water addition (up to 0.1 g H<sub>2</sub>O/g CHP, which is close to the 1:1 mole ratio) the partial molar heat of dilution is constant, suggesting the formation of a CHP hydrate with a heat of formation of -2.4 KJ/mole. At higher water contents, but before the region of the surface tension plateau (the probable micellar range)  $\Delta H_d$  falls sharply. Over the probable micellar range,  $\Delta H_d$  decreases less sharply until entering the fourth region (dilute in CHP, no micelles) where  $\Delta H_d$  falls to zero within the experimental error. The decrease in  $\Delta H_d$  across the micellar range strongly indicates that the micellar aggregates are changing structure and aggregation number on dilution. The value of  $\Delta H_d$  just above the micelle point shows a heat of micelle breakdown corresponding to -9.9 KJ/mole CHP. This large heat of micellization agrees qualitatively with the change of c.m.c. with temperature (Fig. 13).

If it is assumed that both the heat capacity of CHP/water mixtures (Fig. 19) and the  $\Delta H_d$  are constant over the range of experimental temperatures, the osmotic coefficients for CHP in water can be estimated at higher temperatures, and the solute activity coefficients may then be obtained. This procedure was used to calculate the CHP activities shown in Fig. 13 at 22 °C. The calculations were not repeated at 40 °C since the assumptions involved are less valid than at 22 °C.

### *Viscosity*

The viscosity results (Fig. 22) show a maximum viscosity at 25 °C corresponding to a mole ratio of 0.75 CHP/water. The maximum may be further evidence of hydrate formation, though less definite than indicated from the calorimetric data. Hydrates of N-substituted pyrrolidones have been

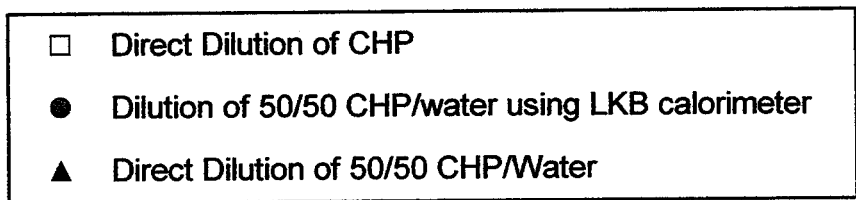
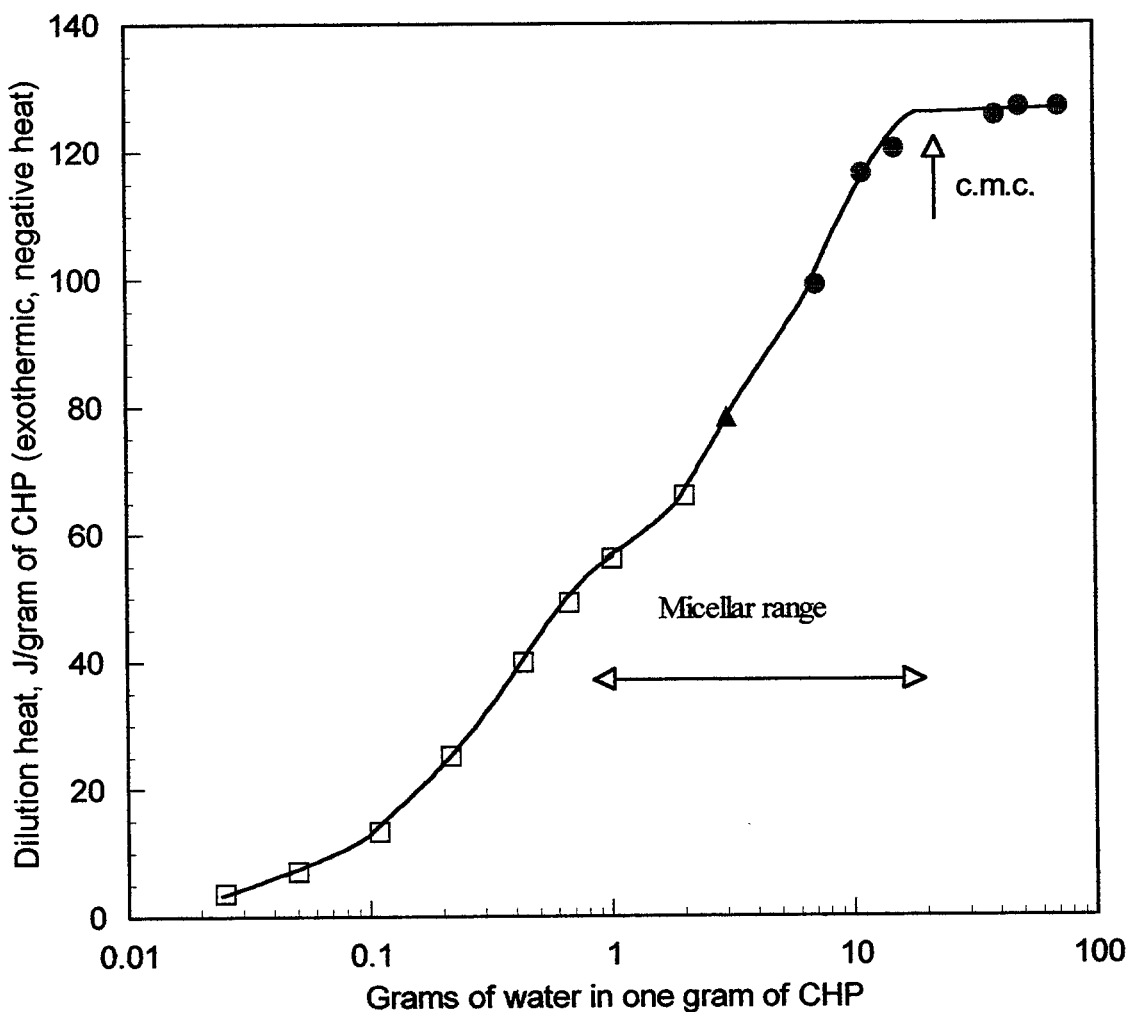
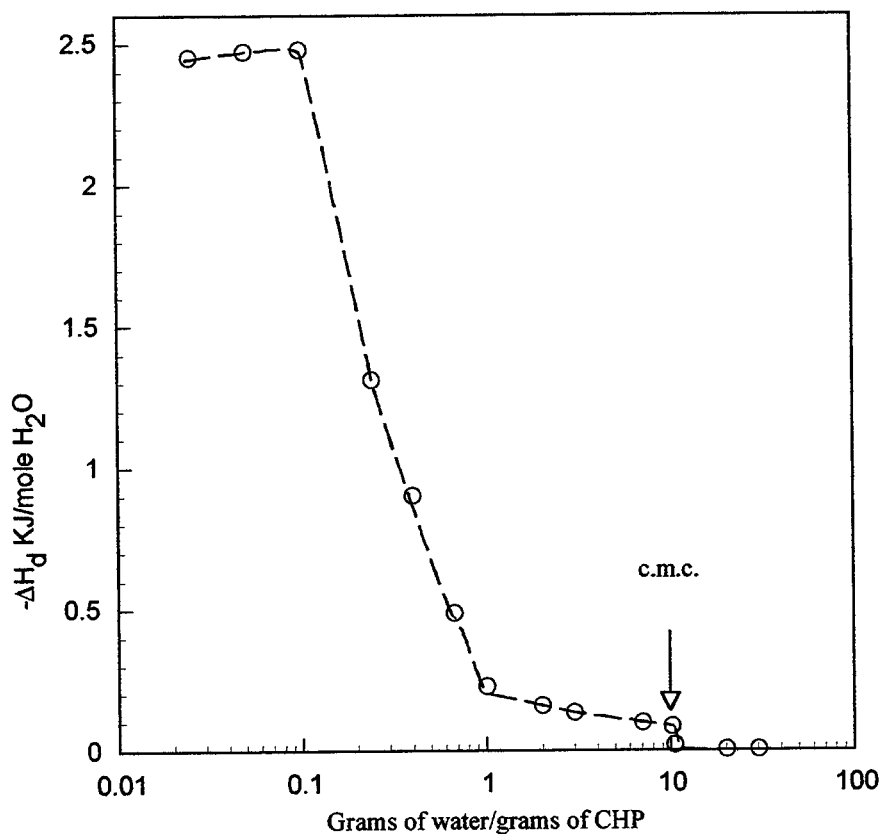


Figure 20. Heat of dilution of cyclohexyl pyrrolidone in water

suggested previously from spectroscopic evidence, but only two such hydrates are known to be sufficiently stable to show clearly on phase diagrams. 2-pyrrole forms a monohydrate with a melting point of 30.4 °C (compared to the melting point of 25 °C for 2-pyrrole itself), and the phase diagram shows two eutectics. N-methyl-2-pyrrolidone (NMP) forms a dihydrate melting at -22 °C, close to

the melting point of NMP, with two clear eutectics in the phase diagram. The spectroscopic evidence for a hydrate of N-vinyl-2-pyrrolidone (VP) was considered, who found only one eutectic in the phase diagram for melting of VP-water mixtures.



**Figure 21. Partial molar heat of dilution of cyclohexyl pyrrolidone in water at the 24 °C**

N-cyclohexyl-2-pyrrolidone (CHP) forms micelles in water at temperatures in the miscibility region below or near the lower consolute temperature. The micelle points are not sharp and the aggregation numbers above but near the c.m.c. increase with temperature from about 5 at 0 °C to about 70 at 40 °C, close to the lower consolute temperature. No “cloud point” phenomenon is observed on approaching the phase boundary. At concentrations well above the c.m.c., the partial molar heats of dilution decrease as the CHP concentration decreases suggesting substantial changes

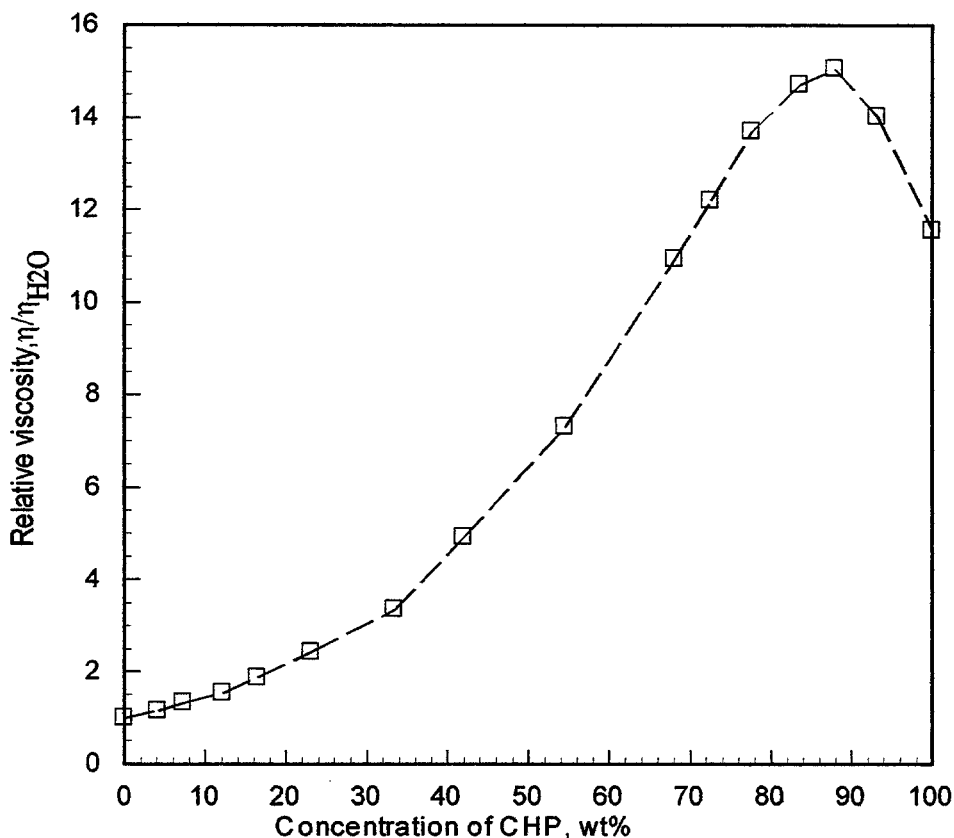


**Figure 22. Relative viscosities of CHP/water mixture at 25 °C**

in micelle structure. The micellar interior resembles pure CHP, as judged from fluorescence measurements with pyrene. CHP is surface active reaching a packing corresponding to  $54 \pm 2$  Å<sup>2</sup>/molecule at high surface pressure. This area is significantly larger than for the n-hexyl analog. From the data at low surface pressures the two-dimensional second virial coefficients at 22 and 40 °C. are shown to be positive but decreasing with temperature, as found for n-alkyl pyrrolidones. The second virial coefficient for the n-hexyl pyrrolidone is negative at 25 °C. This difference is in accord with the finding from the surface tension data that the cyclohexyl ring packs less efficiently on the interface than the n-hexyl compound.

## ADSORPTION OF N-DODECYL- $\beta$ -D-MALTOSE ON VARIOUS HYDROPHILIC SOLIDS

Adsorption isotherms of n-dodecyl- $\beta$ -D-maltoside on hydrophilic solids, alumina, silica, titania and hematite, at neutral pH and 25°C are shown in Figure 23. The surfactant is found to adsorb on alumina, hematite, and titania while it adsorbs of significant less on silica, particularly in the high concentration range.

The adsorption isotherms of n-dodecyl- $\beta$ -D-maltoside on alumina and hematite are very similar and that on titania is somewhat higher. Note that the nature of adsorption, as reflected by the shape of isotherm is markedly different in the case of silica.

A three-stage adsorption phenomenon becomes evident upon examining these isotherms. In the first stage of adsorption, the surfactant adsorbs individually and sparsely on the surface and chain-chain interaction is not significant. A sharp increase in the adsorption density occurs in the second stage, and this is the result of the association of the surfactants into hemimicelles due to the chain-chain interaction. The adsorption isotherm reaches a plateau region at the onset of the third stage. The inflection point between stages II and III corresponds to the critical micelle concentration of the surfactant.

In the plateau region, the adsorption density is about  $5.5 \times 10^{-6}$  mol/m<sup>2</sup> and the surface area per molecule adsorbed is calculated to be 30 Å<sup>2</sup>. Comparing with the value derived from the surface tension at the solution-air interface, which is 48.5 Å<sup>2</sup>, the amount of surfactant adsorbed on the particles is more than that required to form a monolayer and is close to that required for a bilayer. However, this value can be explained equally well by assuming adsorption of surface micelles since a wide range of values can be obtained depending on the shape of adsorbed micelles and its

distribution on the surface.

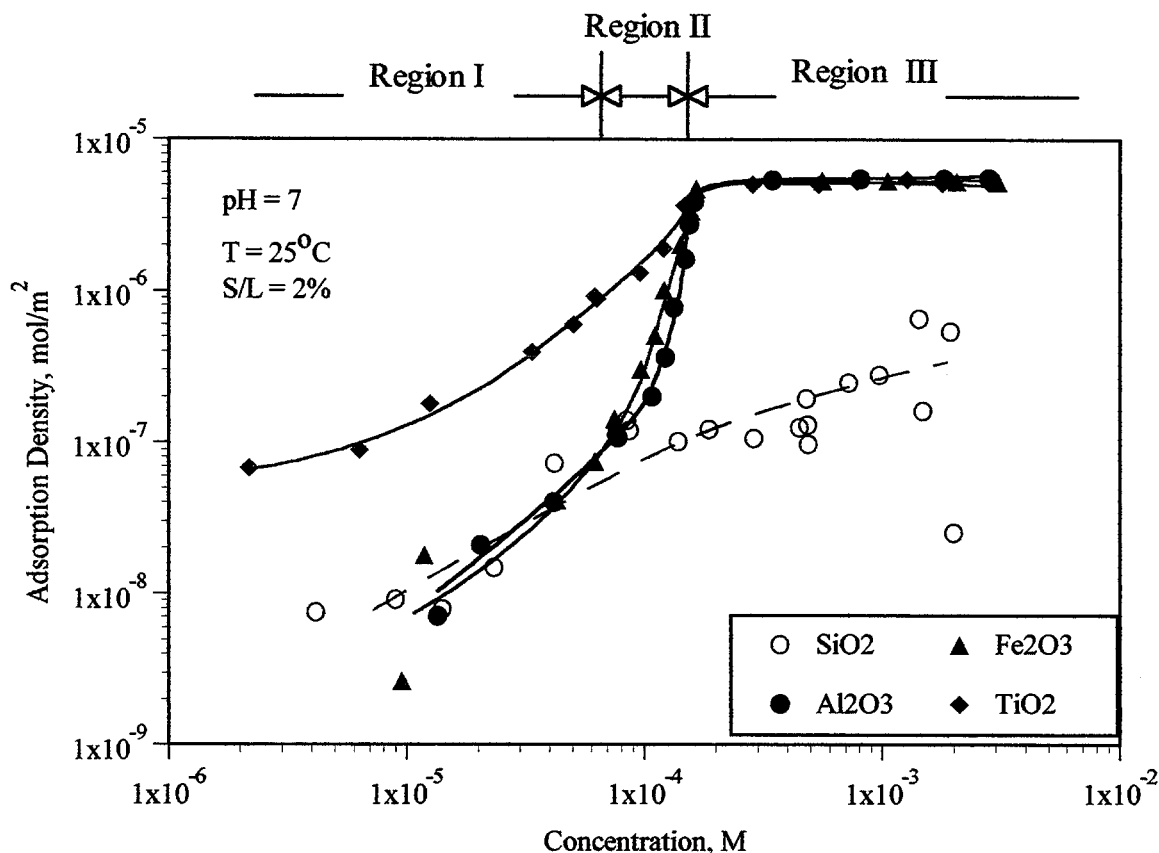


**Figure 23. Adsorption Isotherms of N-Dodecyl-β-D-Maltoside on Hydrophilic Solids**

As indicated above, n-dodecyl-β-D-maltoside adsorbs on alumina, hematite and titania, but much less on silica. Polysaccharide polymers such as dextrin and starch also behave in a similar manner. Another group of nonionic surfactants, the ethoxylates, adsorbs on silica but not on alumina. This drastically different behavior of alkyl polyglucosides surfactants and ethoxylated surfactants may be due to the different interactions between surfactants and solids. Hydrogen bonding has been proposed as the driving force for the adsorption of ethoxylated surfactants on oxides. The adsorption mechanism of alkyl polyglucosides on solids is likely to be different and will be explored in the future.

## ALKYL GLUCOSIDES AND ALKYL MALTOSIDES AT SOLID/LIQUID INTERFACES

### I. Adsorption of Alkyl Glucosides and Alkyl Maltosides on Alumina

To study the effect of important chemical structure variables, the hydrocarbon chain length and the glucose units, on the adsorption of alkyl glucosides and maltosides on solids, adsorption isotherms of octyl, decyl- $\beta$ -D-glucosides and octyl, decyl, dodecyl, tetradecyl- $\beta$ -D-maltosides were determined and the results obtained are shown in Figures 24 and 25. All the isotherms are similar in shape with the inflection point for each surfactant corresponding to its cmc value.

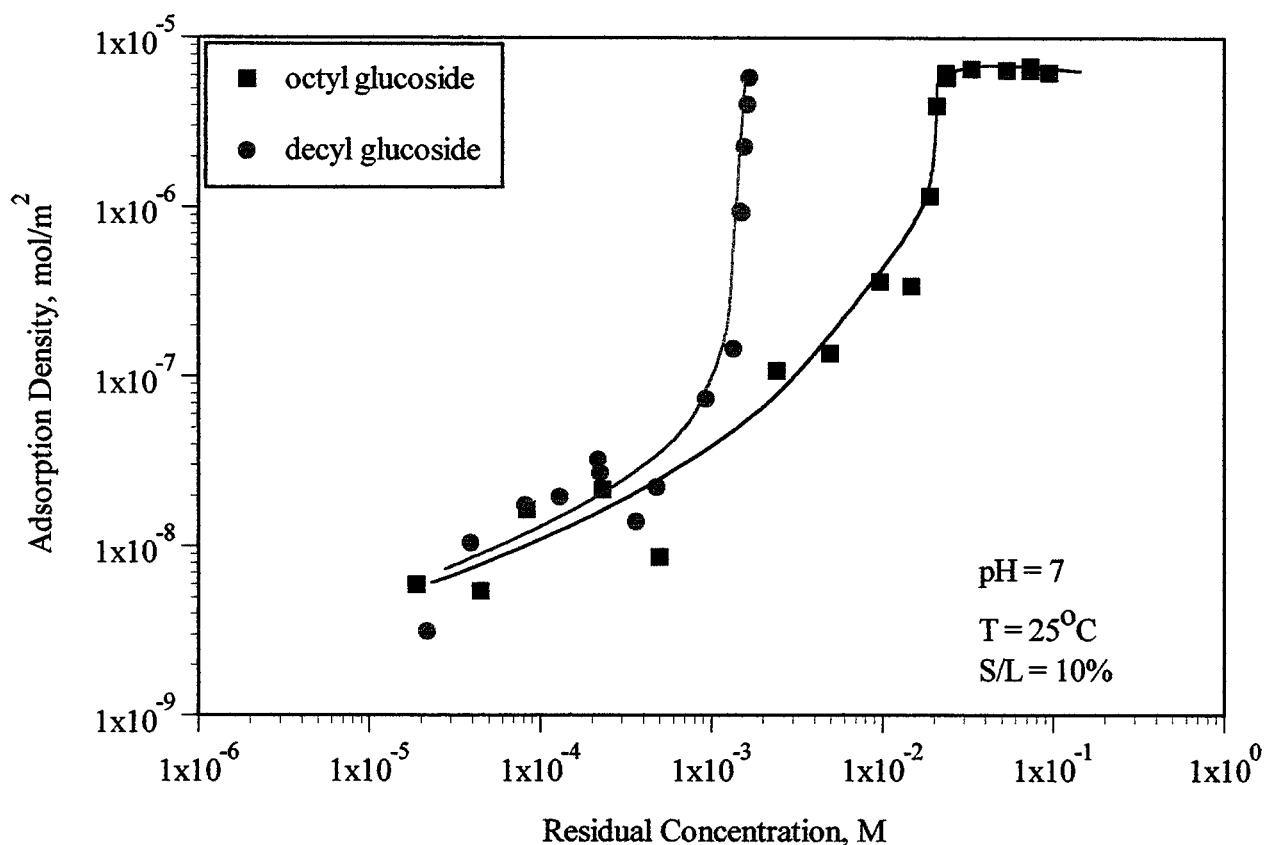
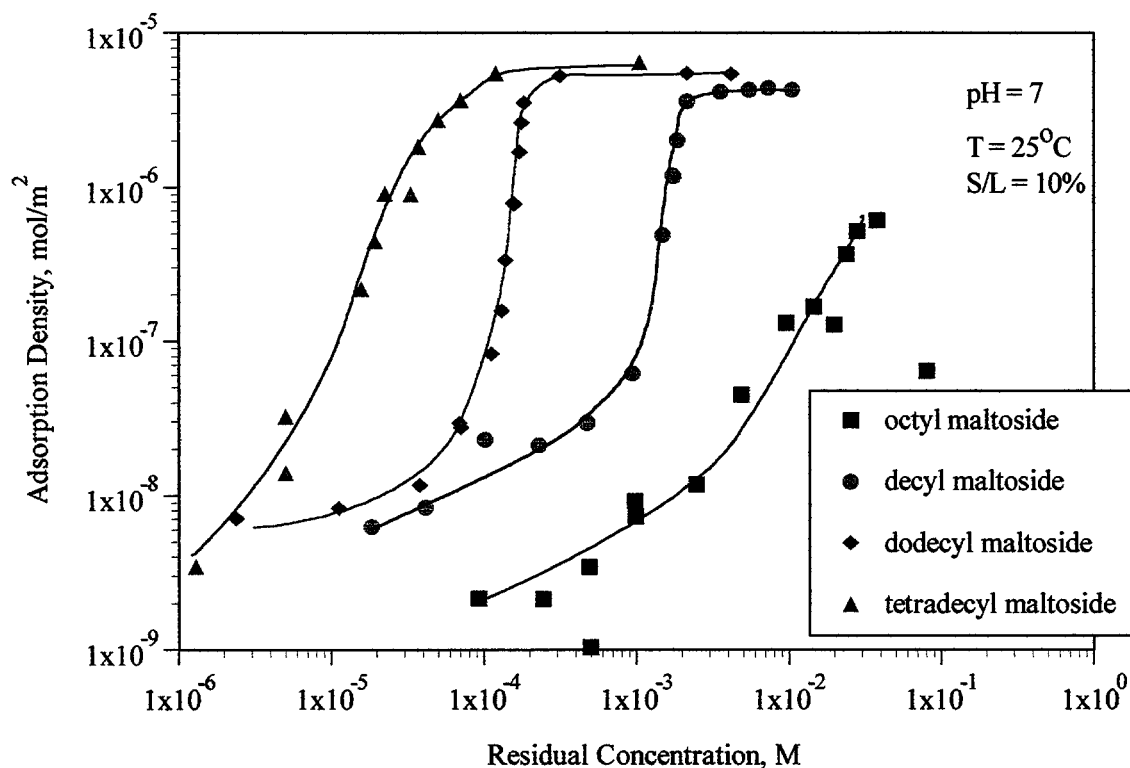


Figure 24 Adsorption of N-Alkyl- $\beta$ -D-Glucosides on Alumina



**Figure 25. Adsorption of N-Alkyl-β-D-Maltosides on Alumina**

It can also be seen from figure 25 that with the chain length increase, there is a small increase in the adsorption density in the plateau region. This suggests that packing for longer chain surfactant is more compact than that for the shorter chain ones, possibly due to the stronger hydrophobic interactions as chain length increases.

Also, glucosides have a higher maximum adsorption density than maltosides of the same chain length. This is due to the small size of glucosides, which requires less area for their packing than maltosides. Furthermore, as the number of glucose units increases, the hydrophobicity of the surfactant is expected to decrease, and this can also cause a decrease in adsorption density of the surfactant. Similar results have been obtained also for ethoxylated surfactants.

The isotherms are analyzed further in-situ to derive fundamental information on the

interactions between the surfactants and the solids.

## II Adsorption Kinetics of *N*-Dodecyl- $\beta$ -D-Maltoside on Alumina

The adsorption kinetics of *n*-dodecyl- $\beta$ -D-maltoside on alumina is shown in Figure 26 for three surfactant concentrations. The adsorption is fast with the process almost complete in 1-2 minutes after the addition of the surfactant. The equilibrium is attained within 30 minutes. This is normal since this surfactant is small and can transport to surface rapidly unless there is a barrier such as that due to electrostatic repulsion.

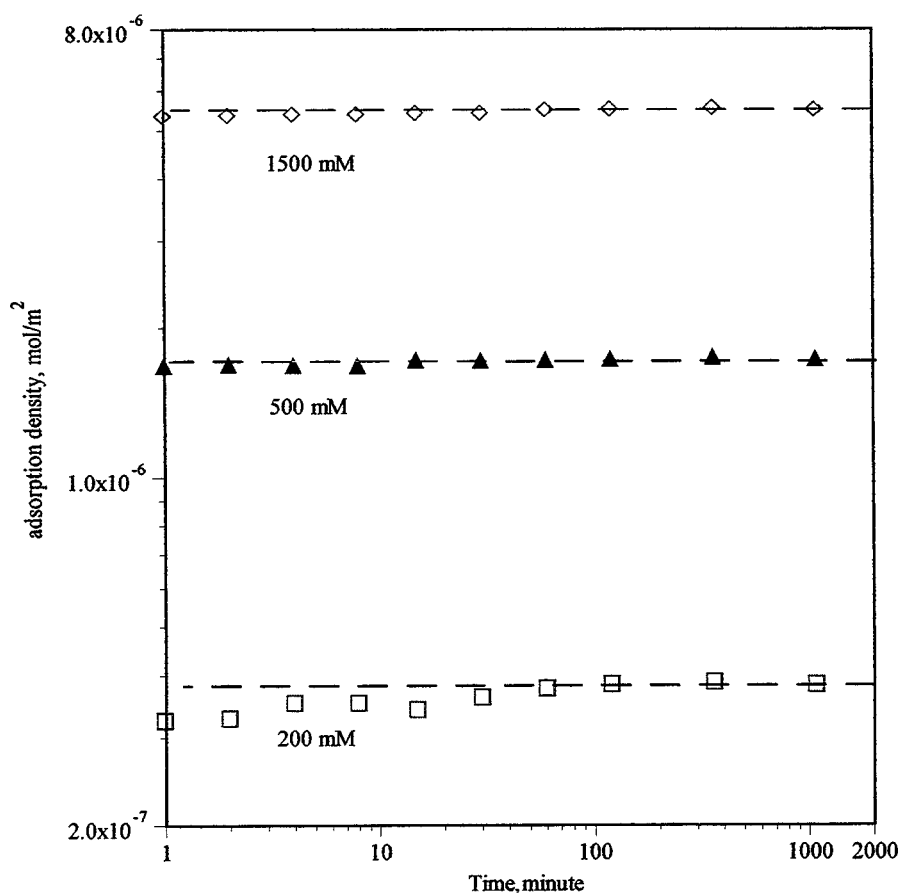


Figure 26. Adsorption Kinetics of *N*-Dodecyl- $\beta$ -D-Maltoside on Alumina

### III. Effect of pH on the N-Dodecyl- $\beta$ -D-Maltoside Adsorption

The effect of pH on the adsorption of DM on alumina is shown in Figure 27. The maltoside adsorption is not affected by the change in pH in the range tested. Since the isoelectric point of AKP-50 alumina is 9, at the two pH conditions tested the zeta-potential of the alumina is very different. The identical adsorption isotherms obtained at the two pH conditions suggest that the electrostatic interaction is not a determining factor for the adsorption of n-dodecyl- $\beta$ -D-maltoside on alumina.

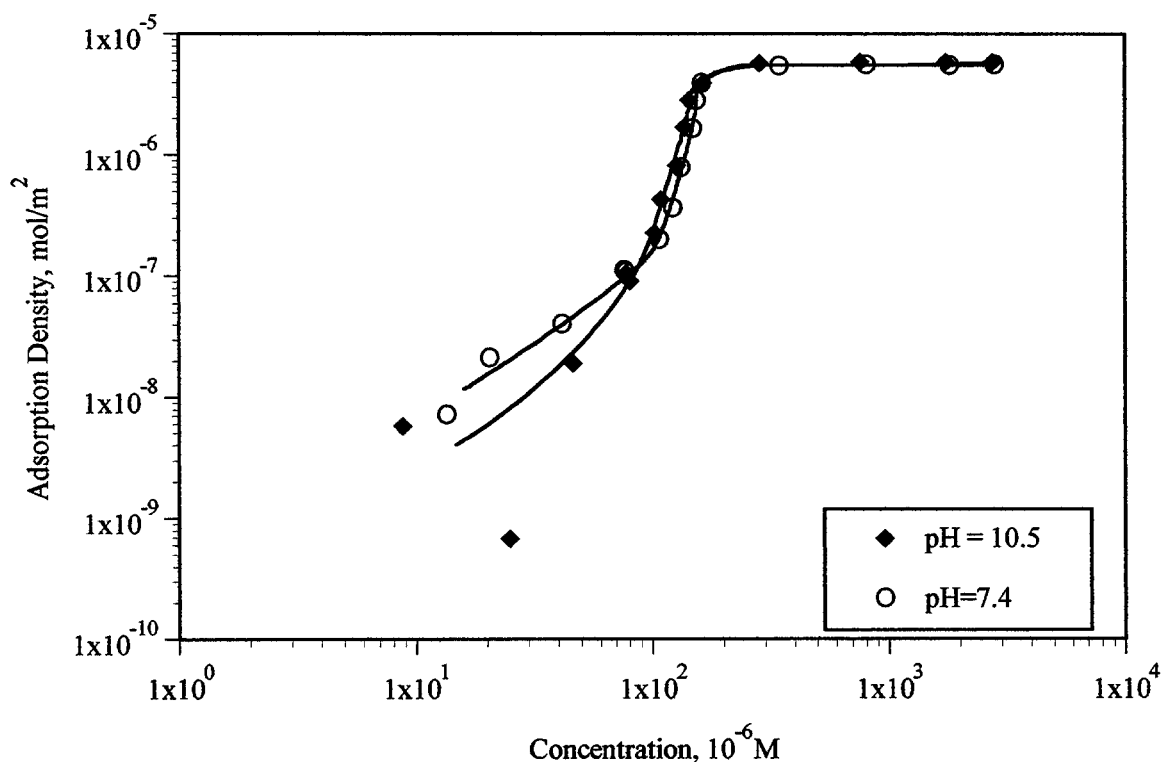


Figure 27. Effect of pH on the Adsorption of N-Dodecyl- $\beta$ -D-Maltoside on Alumina

#### IV. Effect of Salt on the N-Dodecyl- $\beta$ -D-Maltoside Adsorption

The effect of  $\text{Na}_2\text{SO}_4$  salt on the adsorption of n-dodecyl- $\beta$ -D-maltoside on alumina is shown in Figure 28. The adsorption isotherm is found to shift to the left in the lower concentration region and downwards at higher concentrations in the presence of salt. In the present case,  $\text{Na}_2\text{SO}_4$  causes the inflection point to drop from  $1.8 \times 10^{-5}$  mol/L to about  $9 \times 10^{-6}$  mol/L. The surface tension measurements showed that at the same concentration of  $\text{Na}_2\text{SO}_4$ , the cmc of n-dodecyl- $\beta$ -D-maltoside is reduced from  $1.8 \times 10^{-5}$  mol/L to  $9.4 \times 10^{-6}$  mol/L. The effect of salt on surface tension has been attributed to the salting-out of the hydrocarbon chain of the surfactant. The comparable shifting of the inflection point on the adsorption isotherm suggests that the shifting of the adsorption isotherm due to  $\text{Na}_2\text{SO}_4$  can be attributed primarily to changes in solution conditions rather than

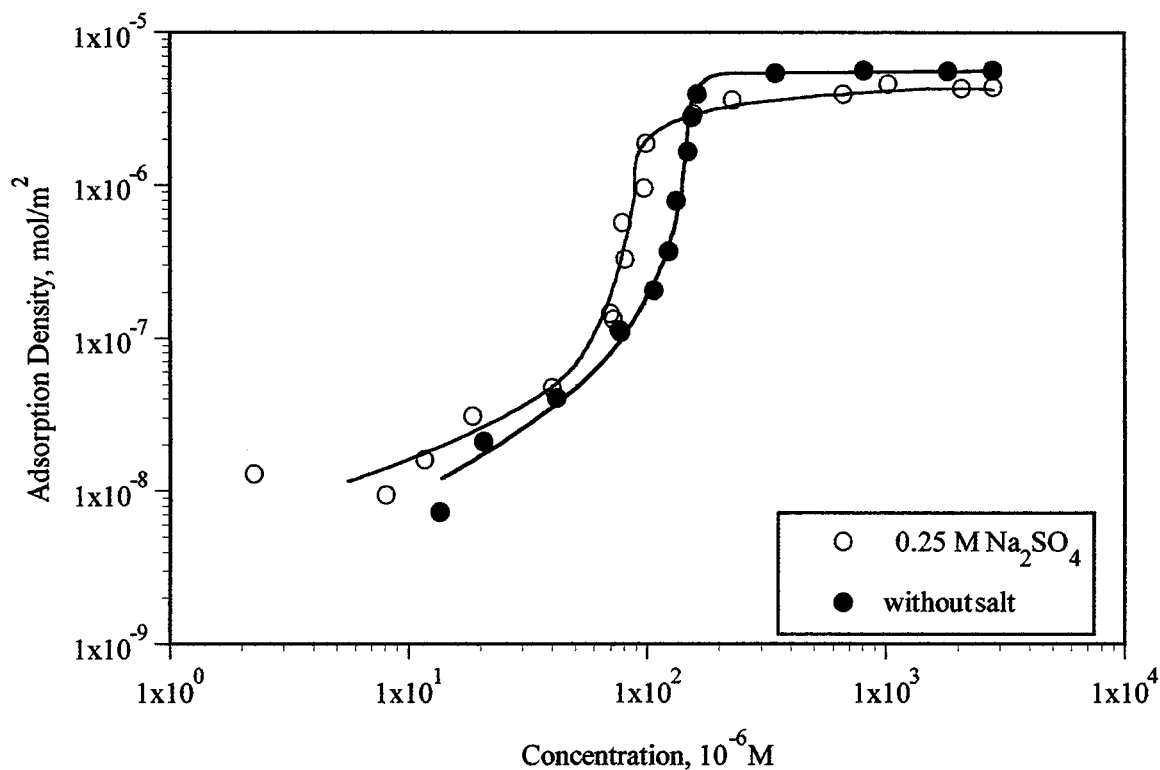


Figure 28. Effect of Salt ( $\text{Na}_2\text{SO}_4$ ) on the Adsorption of N-Dodecyl- $\beta$ -D-Maltoside on Alumina

those on the solid surface. Similar results have been reported for the adsorption of an ethoxylated surfactant on silica in the presence of  $\text{Na}_2\text{SO}_4$ .

#### V. *Fluorescence Spectroscopic Study of N-Dodecyl- $\beta$ -D-Maltoside Adsorption*

To understand the nature of the above adsorption effects, microstructure of the adsorbed layer was probed using fluorescence spectroscopy. The fluorescence of pyrene is very sensitive to the medium in which it resides. The ratio of the intensities of the third and first peaks ( $I_3/I_1$ ) on a pyrene emission spectrum can reveal the polarity of the aggregate environment.

Changes in the polarity parameter of pyrene at the alumina-water interface and in the supernatant are plotted in Figure 29 along with the adsorption isotherm of n-dodecyl- $\beta$ -D-maltoside on alumina. A pyrene spectrum was detected in the solution at all concentrations studied. The polarity parameter changes sharply from  $\sim 0.66$  to  $\sim 1.0$  around the critical micelle concentration of the surfactant, suggesting surfactant aggregate formation in the solution. On the other hand, the pyrene spectrum was seen at the solid-liquid interface only above certain adsorption density. This can be interpreted as due to the beginning of aggregate formation at the solid-liquid interface at this adsorption density. The concentration at which the increase in polarity parameter of surfactant at solid-liquid interface occurs corresponds to the increase in the adsorption density. In the adsorption plateau region, pyrene is present both in the surface aggregates at the solid-liquid interface and micelles in solution. It is reported that in alumina-sodium dodecyl sulfate system, pyrene is preferentially solubilized in solloids at the alumina-water interface rather than in SDS micelles in the supernatant. In contrast, in the alumina-tetradecyl trimethyl ammonium chloride (TTAC) system, pyrene is preferentially solubilized in the micelles than at the solid-liquid interface. The present study suggests that the solubilizing power of DM solloids is between those of SDS and TTAC.

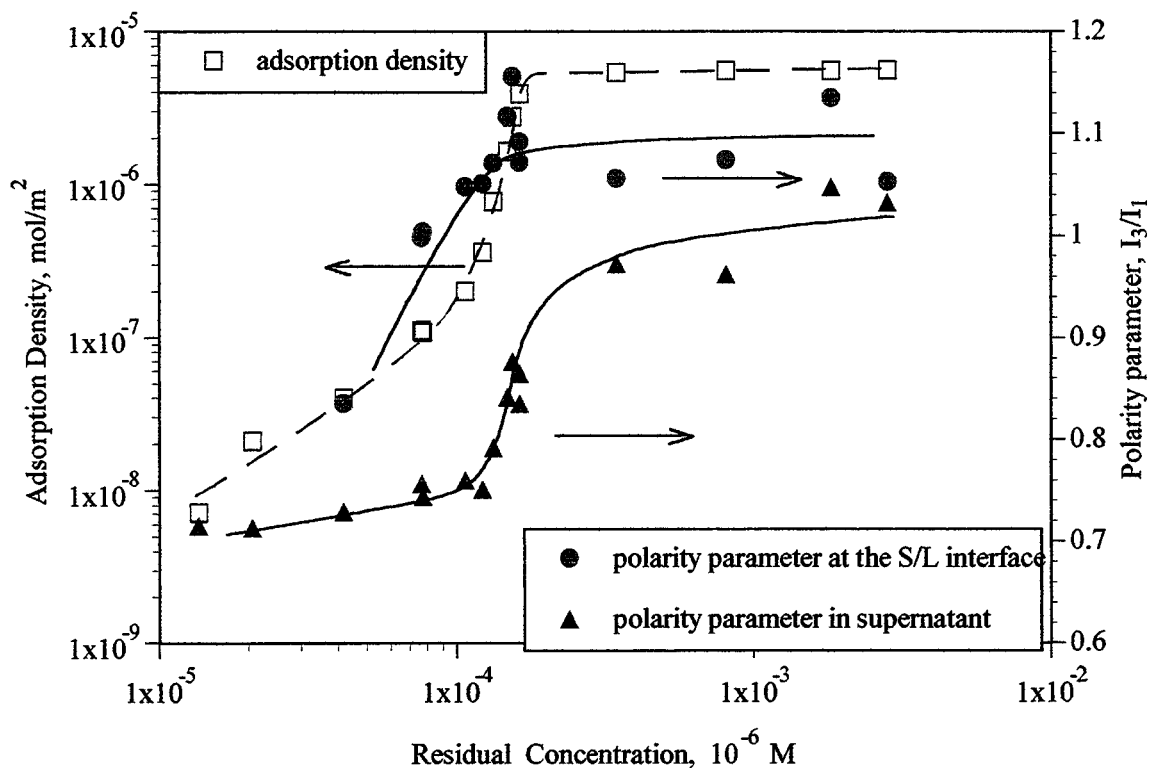


**Figure 29. Polarity parameters of Pyrene at the Alumina/Water Interface and in Supernatant As a Function of N-Dodecyl- $\beta$ -D-Maltoside Adsorption**

In the adsorption plateau region, the polarity parameter of the solloid is higher than that of micelles. This means that packing of surfactants at the solid-liquid interface is denser than that in micelles. This is attributed to the strong hydrophobic chain-chain interaction and inter-penetration of surfactant tails into solloids.

#### VI. Effect of Temperature on the Adsorption N-Dodecyl- $\beta$ -D-Maltoside on Alumina

Adsorption of nonionic surfactant is usually affected by the temperature. For ethoxylated surfactants, due to their dehydration at elevated temperatures, increase in temperature usually causes an increase in adsorption density. Considerable thermodynamic information on adsorption can be obtained by studying the effect of temperature on the adsorption process.

The effect of temperature on the adsorption of n-dodecyl- $\beta$ -D-maltoside on alumina is shown

in Figure 30. It can be seen that temperature has but only a small effect on the adsorption of n-dodecyl- $\beta$ -D-maltoside. The maximum adsorption density is also not affected by the temperature

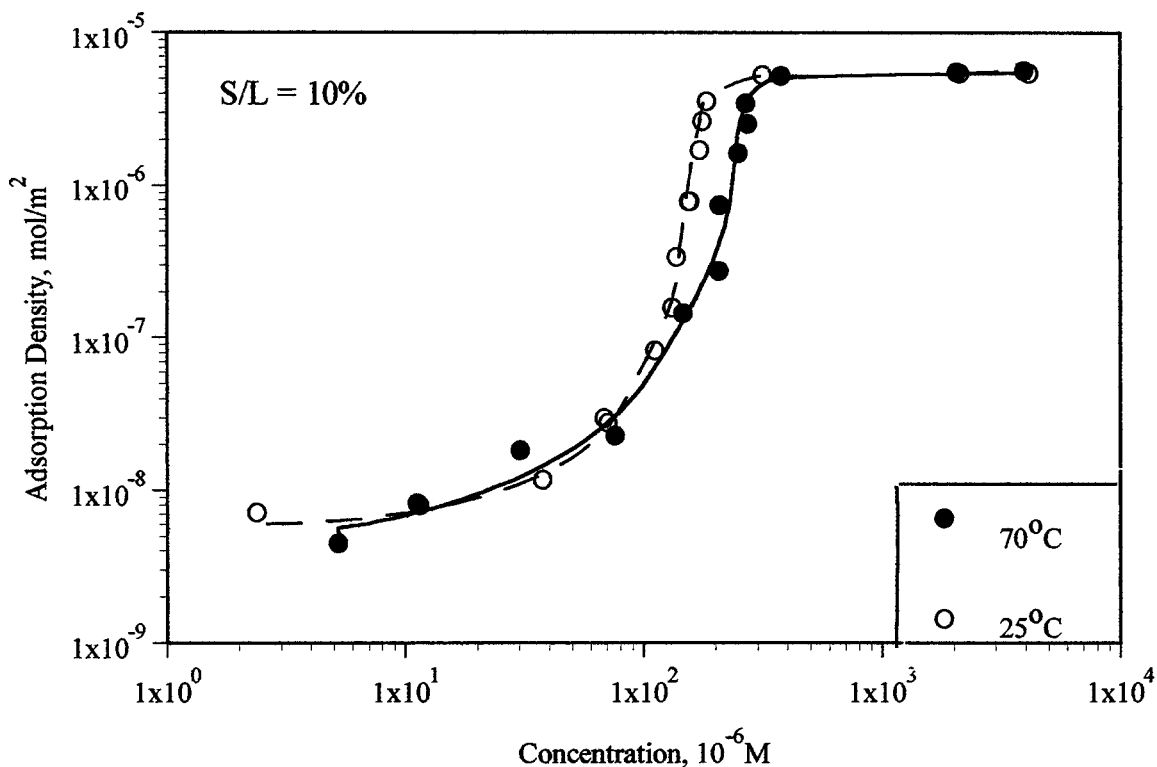


**Figure 30. Effect of Temperature on the Adsorption of N-Dodecyl- $\beta$ -D-Maltoside on Alumina**

change. The shift in inflection point between region II and region III is mostly the result of the increase in critical micelle concentration of the surfactant with an increase in temperature. The small effect of temperature suggests that there is no chemical interaction between the surfactant and the solid.

## VII. *Hydrophobicity of Alumina with N-Dodecyl-β-D-Maltoside Adsorption*

Information on changes in relative hydrophobicity of the solid surface due to surfactant adsorption can give important information on the conformation of the surfactant on the solid and help to elucidate the mechanism involved. The effect of surfactant adsorption on the wettability of the alumina is illustrated in Figure 31 along with the adsorption isotherm. In the absence of the surfactant, the alumina exhibits complete hydrophilicity. With the onset of adsorption on alumina,

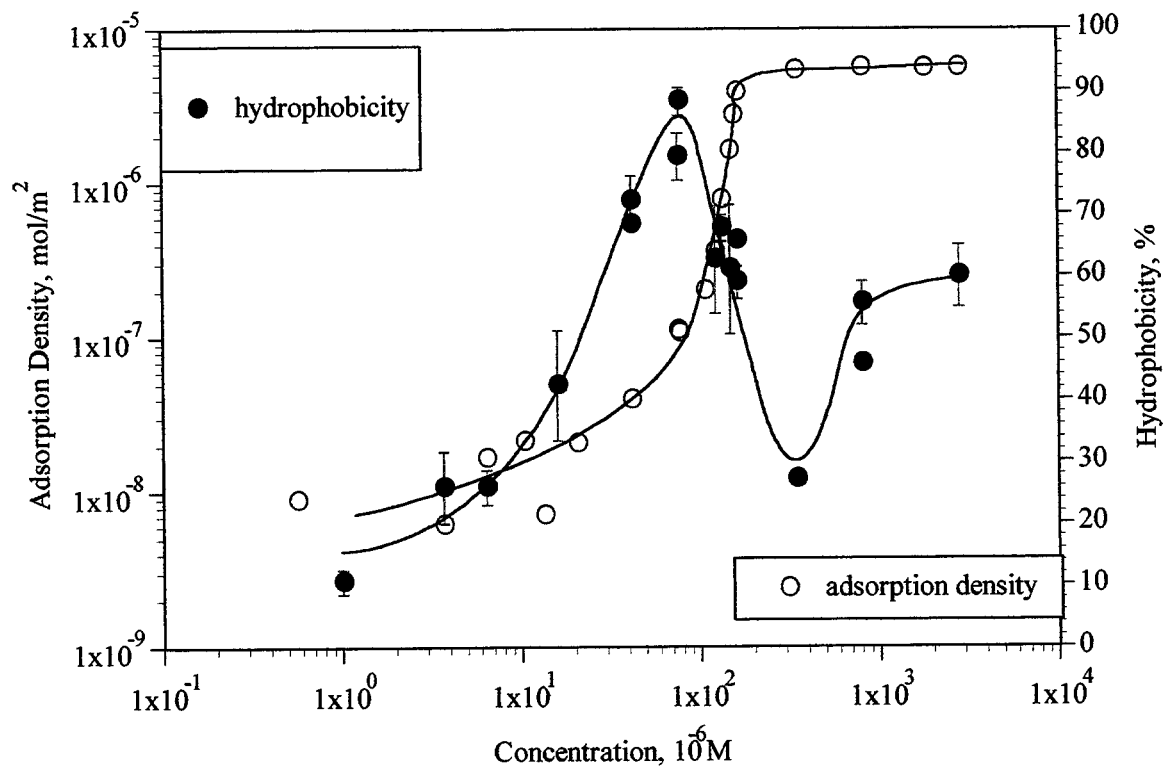


**Figure 31. Adsorption of N-Dodecyl-β-D-Maltoside and Its Effect on the Hydrophobicity of Alumina Particles as Determined by Two Phase Separation**

the surface becomes hydrophobic, suggesting increasing amounts of surfactant to be adsorbing with their hydrophobic tails oriented towards the bulk solution. The hydrophobicity reaches a maximum in the beginning of the region where adsorption density rises sharply. At higher adsorption density

the hydrophobicity decreases. This decrease in hydrophobicity suggests that the chain-chain interaction in this region occurs with some hydrophilic groups orienting towards the aqueous phase. The hydrophobicity of the alumina continues to drop in the region of plateau adsorption. The drop in hydrophobicity in the plateau region is proposed to be due to bilayer adsorption. Further variation in hydrophobicity in the plateau region is possibly related to the effect of high residual DM on the two phase separation that is used here to monitor hydrophobicity.

Similar conclusion can be drawn by examining the hydrophobicity of alumina particles as a function of the adsorption density of n-dodecyl- $\beta$ -D-maltoside(Figure 32). At low adsorption densities, the hydrophobicity of alumina increases with adsorption density and reaches a maximum at the adsorption density of  $10^{-7}$ mol/m<sup>2</sup>. Further adsorption of the surfactant causes the hydrophobicity to decrease, suggesting reverse orientation of the surfactant at the solid/liquid interface.

It is to be noted that the bilayer conformation of n-dodecyl- $\beta$ -D-maltoside on alumina may not be a regular homogenous bilayer. Due to the bulky nature of the maltose head group, close packing of the adsorbed layer will require the hydrocarbon chains of opposing surfactant to interpenetrate each other so that there is actually one layer of hydrocarbon chains with two layers of headgroups on each side. The cross-sectional area of the headgroup is  $48.5 \text{ \AA}^2$  while that of the paraffin chain is about  $20 \text{ \AA}^2$ . Hence the arrangement proposed above can be considered to be a strong possibility.

In summary, adsorption of n-dodecyl- $\beta$ -D-maltoside on hydrophilic solid is proposed to be due to interactions between the solid surfaces and the hydrophilic groups of the surfactant, and at high surfactant concentrations hydrophobic interaction between the surfactant chains .

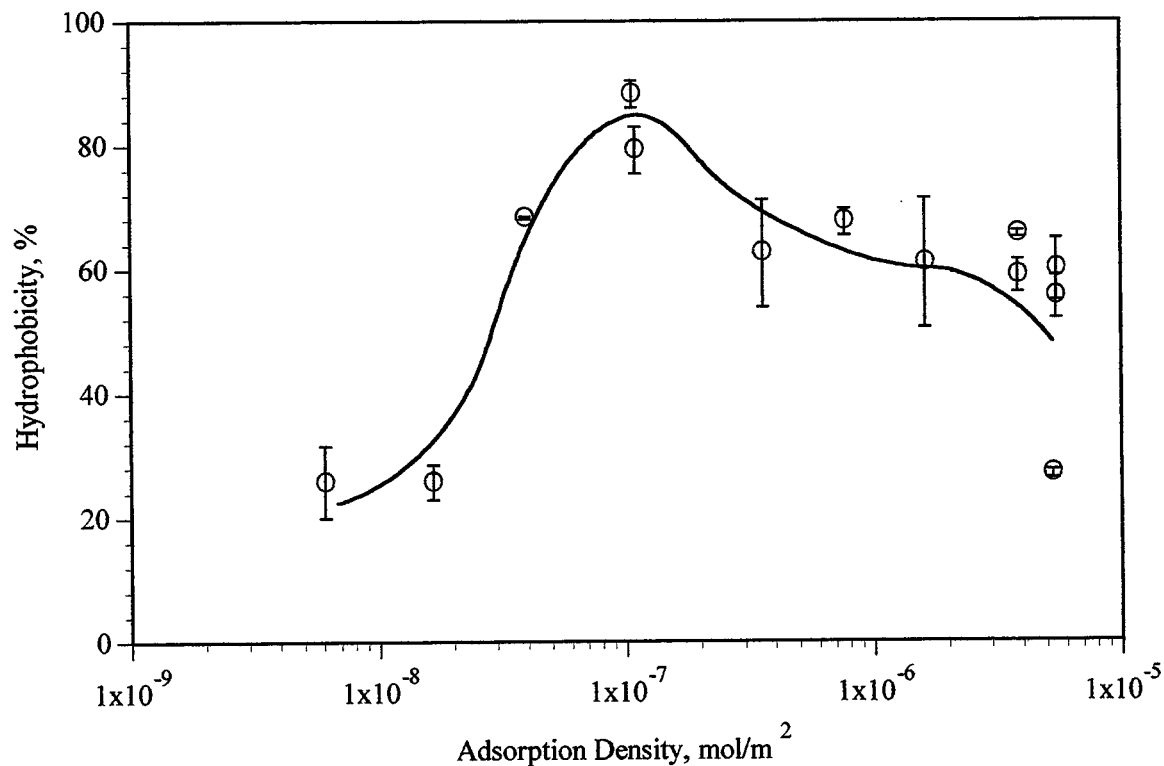


**Figure 32. Hydrophobicity of Alumina Particles after N-Dodecyl- $\beta$ -D-Maltoside Adsorption**

The adsorption of surfactant on hydrophilic solids such as alumina is divided into three regions. At lower concentrations, the surfactant adsorbs on the solid surface individually due to interactions between the surfactant head and the solid surface. At higher concentrations interactions between surfactant chains take place leading to a steep rise in adsorption. Above the cmc of the surfactant the adsorption reaches a plateau. The structure of the saturated adsorbed layer is close to that of a bilayer with hydrophobic chains interpenetrating each other.

The adsorption on hydrophilic solids showed the surfactant to adsorb on alumina, hematite and titania, but much less on silica. The shapes of the adsorption isotherms for alumina, hematite, titania are quite different from that for silica, either. This behavior of alkyl maltoside on hydrophilic

solids is opposite to that of alkyl polyethylene oxide surfactant, and this unique behavior of the sugar-based non-ionic surfactant has practical implications. Effect of salt on the adsorption is attributed to the salting out of the surfactant hydrophobic chain. The adsorption is not affected by the pH changes in the solution. Temperature also has a small effect on the adsorption, suggesting that there is no chemical interaction between surfactant and alumina.

On these solids the final adsorption state is the one in which the surface becomes hydrophilic. This is supported by the results obtained for the wettability and stability changes of the solids upon surfactant adsorption. These properties enable the n-dodecyl- $\beta$ -D-maltoside to be utilized in wetting, oil recovering processes.

## **PUBLICATION**

1. *Brian A. Pethica, Zhenghe Zhu, Anjing Lou and P. Somasundaran*, "Surface and Colloidal Properties of Cyclic Amides. 4. N-cyclohexyl-2-pyrrolidone/water Mixtures Aggregation in solution and adsorption at the air/solution interface" Submitted to Langmuir.
2. P. Somasundaran and L. Huang, "Adsorption/aggregation of Surfactants And Their Mixtures at Solid-liquid Interfaces" Submitted to Advances in Colloid and Interface Science.
3. P. Somasundaran and L. Huang, "Adsorption of Polymers at Solid-liquid Interfaces" Submitted for the book entitled "Polymer in Personal Care, Pharmaceutical, and Industrial Applicatin", To be published by Marcel Dekker Inc..